4

CENTRAL RESEARCH LIBRARY
DOCUMENT COLLECTION

MARTIN MARIETTA ENERGY SYSTEMS LIBRARIES
3 4456 0350329 7

ORNL-2193
Physics and Mathematics

Cy. 4

RADIATION ATTENUATION CHARACTERISTICS OF STRUCTURAL CONCRETE

E. P. Blizard
J. M. Miller

CENTRAL RESEARCH LIBRARY
DOCUMENT COLLECTION
LIBRARY LOAN COPY
DO NOT TRANSFER TO ANOTHER PERSON
If you wish someone else to see this document, send in name with document and the library will arrange a loan.

OAK RIDGE NATIONAL LABORATORY
operated by
UNION CARBIDE CORPORATION
for the
U.S. ATOMIC ENERGY COMMISSION

Printed in USA. Price 1.50 cents. Available from the

Office of Technical Services
U. S. Department of Commerce
Washington 25, D. C.

LEGAL NOTICE

This report was prepared as an account of Government sponsored work. Neither the United States, nor the Commission, nor any person acting on behalf of the Commission:

A. Makes any warranty or representation, express or implied, with respect to the accuracy, completeness, or usefulness of the information contained in this report, or that the use of any information, apparatus, method, or process disclosed in this report may not infringe privately owned rights; or

B. Assumes any liabilities with respect to the use of, or for damages resulting from the use of any information, apparatus, method, or process disclosed in this report.

As used in the above, "person acting on behalf of the Commission" includes any employee or contractor of the Commission to the extent that such employee or contractor prepares, handles or distributes, or provides access to, any information pursuant to his employment or contract with the Commission.

ORNL-2193

Copy No. 4

Contract No. W-7405-eng-26

APPLIED NUCLEAR PHYSICS DIVISION

RADIATION ATTENUATION CHARACTERISTICS OF STRUCTURAL CONCRETE*

E. P. Blizard and J. M. Miller

DATE ISSUED

AUG 13 1958

OAK RIDGE NATIONAL LABORATORY
Oak Ridge, Tennessee
operated by
UNION CARBIDE CORPORATION
for the
U. S. ATOMIC ENERGY COMMISSION

*An expanded version of data previously published in ORNL-2081, p. 157 (1956).

MARTIN MARIETTA ENERGY SYSTEMS LIBRARIES

3 4456 0350329 7

ABSTRACT

An experiment was performed at the Lid Tank Shielding Facility to determine the dependence of the neutron attenuation of a structural concrete shield on the amount and placement of water hydrogen throughout the shield. It was found that a 7 wt% water content is adequate to insure that intermediate-energy neutrons are quickly slowed down to thermal energy, at which energy they are easily captured. A greater water content improves the over-all neutron attenuation according to the removal cross-section theory. In addition to the investigation of the neutron attenuation, the measured gamma-ray attenuation was compared with the predicted gamma-ray attenuation obtained in a calculation using buildup factors determined by the moments method. The two values were in good agreement.

ACKNOWLEDGEMENTS

The authors would like to express their appreciation to G. T. Chapman who assumed much of the responsibility for the design and performance of the experiment.

TABLE OF CONTENTS

		Page
	Abstract	iii
	Acknowledgements	iii
	Introduction	1
I.	Experimental Apparatus and Procedure	2
II.	Experimental Results and Discussion	7
	Neutron Attenuation	7
	Experimental Results	8
	Analysis	8
	Gamma-Ray Attenuation	26
App. A.	Tabulation of Radiation Measurements Beyond the Configurations	38
App. B.	List of Figures	46

INTRODUCTION

By virtue of its low unit price, concrete of some type is nearly always used for stationary reactors where the thickness and weight of the shield are not critical factors. In general, the effectiveness of a concrete shield of a certain design has been predicted by calculating the gamma-ray attenuation of the shield by the moments method[1] and the fast-neutron attenuation by the removal cross-section concept.[2] However, for the latter concept to apply, sufficient moderator and absorber must be present in the shield to slow the scattered fast neutrons down without excessive further travel to thermal energy, at which they are easily captured.

It has generally been assumed that it is necessary to add hydrogen to the shield to slow down the neutrons to thermal energy in a short distance. It was feared that without this added hydrogen the fast neutrons would be slowed down only to intermediate energies at which energies they would diffuse through the shield, as has been observed in the case of pure iron,[3] since their energies are too great for them to be captured and too low for them to be inelastically scattered. There has, however, been some question about the necessity of adding the hydrogen since there is a considerable amount of oxygen in a concrete shield and its slowing-down effect by elastic scattering alone might well be sufficient.

In order to obtain experimental information with which this question could be resolved, a series of tests has been performed at the Lid Tank Shielding Facility (LTSF). The shield mockups used for the tests consisted of various configurations of structural concrete and water. The amount and placement of the water (used here as a vehicle for hydrogen) was varied, and the radiation levels in water beyond the mockups were measured. The results of the experiment and subsequent analysis are presented in this report.

In addition to the study of the neutron attenuation, the measured gamma-ray attenuation was compared with that predicted by calculation.

---

1. Herbert Goldstein and J. Ernest Wilkins, Jr., "Calculations of the Penetration of Gamma Rays," NYO-3075 (June 30, 1954).

2. R. D. Albert and T. A. Welton, WAPD-15 (Nov. 30, 1950) (Classified); see also E. P. Blizard, "Procedure for Obtaining Effective Removal Cross Sections from Lid Tank Data," ORNL-CF-54-6-164 (June 22, 1954) (Declassified, 1955); see also G. T. Chapman and C. L. Storrs, "Effective Neutron Removal Cross Sections for Shielding," ORNL-1843 (Aug. 31, 1955) (Declassified, 1956).

3. E. P. Blizard, G. T. Chapman, and J. D. Flynn, "A Comparison of the Streaming of Thermal Neutrons Through Iron and Stainless Steel in the ORNL Lid Tank," ORNL-CF-53-6-186 (1953).

I. EXPERIMENTAL APPARATUS AND PROCEDURE

The LTSF is a 7 by 7 by 11 ft tank of water which acts as a "lid" to a hole through the 7-ft-thick concrete shield of the ORNL Graphite Reactor. This hole is rectangular in cross section, increasing in three steps from 23-1/2 by 27-1/2 in. at the inside to 28 by 32 in. at the outside. There is a 28-in.-dia uranium converter plate at the outside of the hole which serves as the radiation source for the facility. This plate consists of an array of natural uranium slugs (1.1 in. in diameter and 4 in. long), which are activated by thermal neutrons from the reactor to produce a fission source.

An additional steel tank was used in the experiment to contain the concrete slabs to be tested. This tank, which had 5/8-in.-thick walls, was placed inside the "lid" tank as close to the fission source as was physically possible. Because steel is known to produce high-energy capture gamma rays, a 30-in.-square hole was cut in the side of the tank adjacent to the source, and a 3/8-in.-thick sheet of aluminum, which is not a strong capture gamma-ray producer, was then bolted over it. The unavoidable 2.3-cm space between the source and the window was filled with an air-inflated plastic bag. For some configurations a second tank was required which was placed inside the steel tank. This tank was aluminum and had 1/8-in.-thick walls.

The concrete used in the configurations consisted of 2-in.-thick slabs, 56 in. high by 64 in. wide. Each slab was amercoated (a patented waterproof paint) to prevent absorption of water during the experiment. The analysis of the concrete, which had an average density of 2.39, is given in Table 1.

Table 1. Chemical Analysis of the Concrete Tested at the LTSF[a]

Constituent	Concentration (wt%)	Constituent	Concentration (wt%)
Loss on ignition	25.32	K	0.18
Insoluble residue[b]	30.51	Ca	24.33
SO_3	0.73	Mg	2.40
SiO_2	30.63	H	0.83
Fe_2O_3	1.57	C	4.92
Al_2O_3	6.68	O	46.7
P	0.31	Al	3.54
Mn	0.11	Si	14.3
CO_3	24.62	S	0.29
H_2O[c]	7.48	Fe	1.10
Na	0.45		

a. Density = 2.39 g/cm; analyses based on three samples.
b. Insoluble in HCl.
c. Includes water of hydration.

Three types of configurations were used: (1) dry configurations where slabs in flush positions were contained in a water-exclusion or "dry" tank, (2) wet configurations where slabs in flush positions were placed in water, and (3) laminated configurations where the slabs were spaced out in water. The configurations tested are described in Table 2 and shown in Fig. 1. Because some of the slabs were slightly bowed, there were spaces between them even when "flush." The total space (air or water) distributed throughout each configuration (see Table 3) was determined by assuming that each slab was exactly 2 in. thick and subtracting the total concrete thickness from the total measured configuration thickness. This assumption of uniform slab thickness is considered valid since the rectangular dimensions of the slabs were the same and the weights of the slabs (with frames) were essentially the same (see Table 4).

Measurements of the attenuation of the fast-neutron dose rate, the thermal-neutron flux, and the gamma-ray dose rate were made along the horizontal axis of the source in the water beyond the concrete. A Hurst dosimeter[4] was used to measure the fast-neutron dose rate. Thermal-neutron flux measurements were made with a 12-1/2-in. BF_3 proportional counter,[5] as well as with two fission chambers (3- and 1/2-in.-dia U^{235} plates, respectively). The gamma-ray dose rate measurements were made with a 900-cc graphite-lined ionization chamber.[6] The results of the measurements are presented and discussed in Section II.

---

4. G. S. Hurst and R. H. Ritchie, "A Count-Rate Method of Measuring Fast Neutron Tissue Dose," ORNL-930 (Jan. 30, 1951).

5. B. B. Rossi and H. H. Staub, "Ionization Chambers and Counters; Experimental Techniques," McGraw-Hill, New York, 1949.

6. L. H. Ballweg and J. L. Meem, "A Standard Gamma-Ray Ionization Chamber for Shielding Measurements," ORNL-1028 (July 9, 1951).

Table 2. Description of Concrete Configurations Tested at LTSF[a]

Configuration No.	Description
0	A water-filled steel tank with $\frac{3}{8}$-in.-thick Al window on the source side was placed in the water of the LTSF; the 2.3-cm space between the Al window and the source was filled with air contained in a plastic bag
1	An Al tank ($\frac{1}{8}$-in.-thick walls) filled with 19 dry 2-in.-thick concrete slabs was placed inside the steel tank; the $\frac{3}{8}$-in. space between the Al window of the outer tank and the Al wall of the inner tank was filled with water
2	13 dry 2-in.-thick concrete slabs were placed inside the steel tank; the $\frac{3}{8}$-in. space between the Al wall and the first slab was filled with air; the water-filled Al tank was positioned behind the concrete
3	Same as configuration 2 except concrete slab section was flooded with water
4	Same as configuration 3 except Al tank was removed
5	Same as configuration 4 but with $\frac{1}{8}$-in.-thick water gaps between slabs
6	Same as configuration 4 but with $\frac{1}{2}$-in.-thick water gaps between slabs
7	Same as configuration 4 but with $\frac{1}{4}$-in.-thick water gaps between slabs
8	2 adjacent slabs in water-filled steel tank
9	4 adjacent slabs in water-filled steel tank
10	Same as configuration 8 but 6 slabs were used
11	Same as configuration 8 but 8 slabs were used
12	Same as configuration 8 but 12 slabs were used
13	Same as configuration 8 but 16 slabs were used
14	Same as configuration 8 but 19 slabs were used
15	Same as configuration 8 but 22 slabs were used
16	2 adjacent slabs followed by $\frac{1}{2}$-in.-thick water followed by 2 adjacent slabs followed by $\frac{1}{2}$-in. water gap, etc. for a total of 22 slabs
17	Same as configuration 16 except for a total of 20 slabs
18	Same as configuration 16 except for a total of 18 slabs
19	Same as configuration 16 except for a total of 16 slabs
20	Same as configuration 16 except for a total of 12 slabs
21	Same as configuration 16 except for a total of 8 slabs
22	Same as configuration 16 except for a total of 6 slabs
23	Same as configuration 16 except for a total of 4 slabs

[a]See also, Fig. 1.

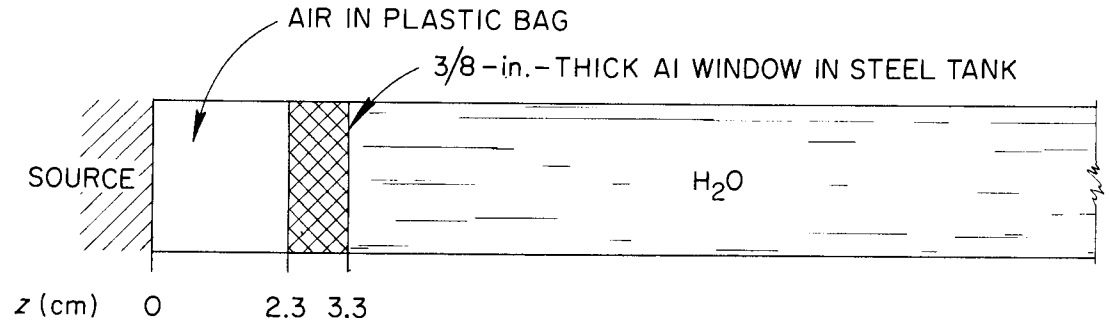

CONFIGURATION 0

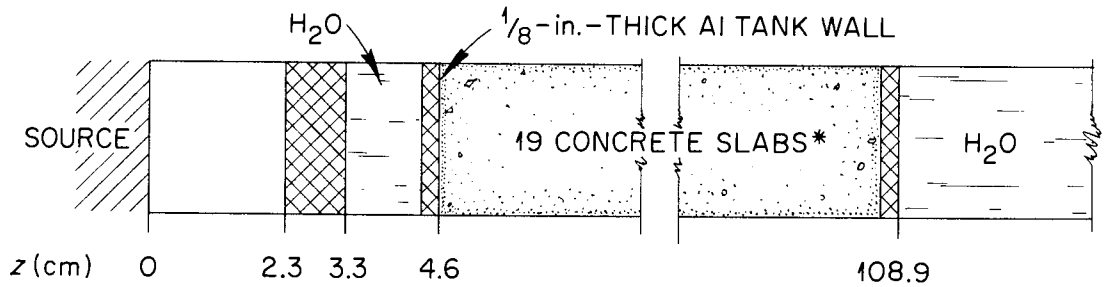

CONFIGURATION 1

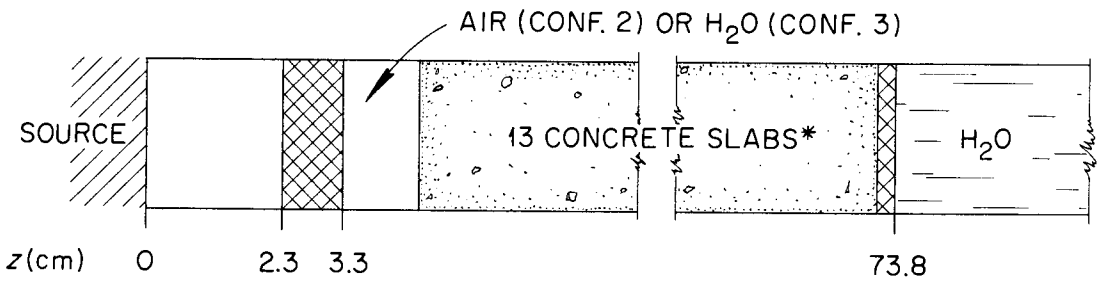

CONFIGURATIONS 2 AND 3

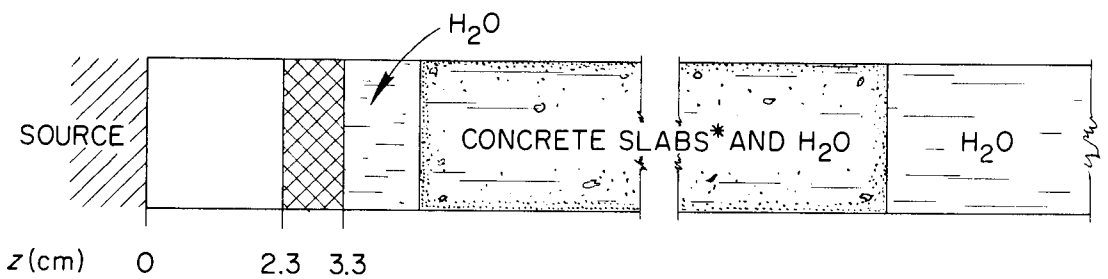

CONFIGURATIONS 4 THROUGH 23
(SEE TABLE 1)

*2 in. THICK

Fig. 1. Concrete Configurations Tested at the LTSF.

Table 3. Water, Air, and Aluminum Thicknesses in the Various Configurations

onf. No.	Thickness[a] (cm)	No. of Slabs	Equivalent Thickness of Water in Slabs (cm)[b]	Thickness of Water Between Slabs (cm)	Total Water[c]	Other Materials (cm)
1	105.6	19	17.3	0.0	18.3	0.6 Al, 7.5 Air
2	70.5	13	11.8	0.0	11.8	0.3 Al, ~4 Air
3	70.5	13	11.8	3.2	16.0	0.3 Al
4	71.3	13	11.8	4.2	17.0	
5	74.3	13	11.8	7.2	20.0	
6	86.5	13	11.8	19.4	32.2	
7	78.0	13	11.8	10.9	23.7	
8	11.3	2	1.8	0.1	2.9	
9	22.4	4	3.6	1.4	6.0	
10	33.7	6	5.4	2.2	8.6	
11	45.8	8	7.3	4.2	12.5	
12	66.6	12	10.9	4.4	16.3	
13	89.6	16	14.5	7.3	22.8	
14	106.0	19	17.3	8.5	26.8	
15	123.8	22	20.0	10.9	31.9	
16	135.7	22	20.0	22.8	43.8	
17	122.8	20	18.2	20.0	39.2	
18	109.6	18	16.4	17.1	34.5	
19	97.5	16	14.5	15.2	30.7	
20	73.0	12	10.9	11.0	22.9	
21	50.6	8	7.3	9.0	17.3	
22	36.9	6	5.4	5.4	11.8	
23	24.3	4	3.6	3.0	7.6	

a. All configurations have 2.3 cm of air plus 1 cm of Al in addition to the thicknesses given in columns 5 - 7.

b. Includes water of hydration.

c. Includes 1 cm of water between first slab and source plate on all wet configurations.

Table 4. Weights of Concrete Slabs (with Frames)[a]

Slab No.	Weight (lb)	Slab No.	Weight (lb)	Slab No.	Weight (lb)
1	659	9	671	16	651
2	657	10	664	17	659
3	676	11	667	18	642
4	675	12	648	19	662
5	698	13	666	20	676
6	674	14	666	21	655
7	671	15	672	22	670
8	685				

a. Weight of frames = 67 lb.

II. EXPERIMENTAL RESULTS AND DISCUSSION

Neutron Attenuation

As stated previously, the primary purpose of this investigation has been to determine whether ordinary concrete shields moderate the scattered fast neutrons well enough for the fast-neutron removal cross section concept to describe the attenuation reasonably well. The cross section for fast neutrons (several Mev and above) is in general smaller than that for neutrons of intermediate or low energies, so that they must be the most difficult to attenuate. In case, however, the materials of the shield do not contain sufficient quantities of light (low atomic weight) elements, the intermediate-energy neutrons, being of too low energy to be inelastically scattered, and too high to be absorbed, may undergo many elastic scatterings with little moderation, and hence penetrate the shield. This situation can be avoided in the case of concrete by the addition of water, which because of its hydrogen is a good moderator, with relatively less effect on the attenuation of fast neutrons or gamma rays. With adequate moderation the shield will then exhibit an attenuation of neutrons characteristic of the fast-neutron attenuation, which is described by an exponential function with the fast-neutron macroscopic removal cross section for the attenuation coefficient. This experiment has been carried out to find the fast- and intermediate-neutron attenuation of ordinary concrete and from this to determine whether it is necessary to take steps to add extra water to an ordinary concrete reactor shield.

Unfortunately, the available neutron detectors are not sufficiently sensitive to intermediate-energy neutrons,* so it was necessary to design the experiment so that penetrating neutrons in this energy region could be estimated from the thermal-neutron flux distribution in a region of water following the concrete. Water can be used as a rough spectrometer. Since diffusion at thermal energies is small for neutrons in water, the thermal-neutron flux is a good indicator of faster neutrons slowed down in the

---

*The Hurst dosimeter (recoil-proton dosimeter) is not a reliable instrument in the intermediate-energy range as its energy cutoff must be set high enough to suppress a response to gamma rays. This cutoff energy is usually set at 200 kev.

vicinity. Attenuation of leaking neutrons in water, as indicated by the thermal-neutron flux, varies strongly with neutron energy because of the variation in hydrogen cross section. Thus, for example, in Fig. 2, it is possible to see in the water close to the concrete a region in which the attenuation rate is large (relaxation length = 4.5 cm) indicating the presence of neutrons of intermediate to low energy. At larger distances ($>$60 cm) the attenuation rate is much less (relaxation length = 9.8 cm), indicating quite fast ($\sim$8-Mev) neutrons. These phenomena will be used in analyzing the performance of the concrete as a neutron shield.

Experimental Results

In the experiment, measurements of the thermal-neutron flux were made in the water following the concrete as a function of the distance (up to 160 cm) from the source. The results, which are plotted in Figs. 2 through 5, not only show the effect of increasing the total thickness of adjacent concrete slabs in a water or air medium, but also the effect of introducing water gaps throughout the shields. These measurements were cross plotted (Figs. 6 and 7) as a function of the total thickness of concrete for fixed distances of 15 and 30 cm beyond the shield. In addition, fast-neutron measurements were taken in an overlapping region between 50 and 110 cm. These are shown in Figs. 9 through 11.

Analysis

The attenuation of fast neutrons in a shield can be attributed to three successive processes: (1) collision, either inelastic or elastic and involving significant change of direction or energy degradation or both (elastic forward scattering attenuates very little); (2) slowing down by many collisions, mostly elastic; and (3) diffusion at or near thermal energy to absorption. The characteristic length associated with process (1) is the fast-neutron removal attenuation length, the reciprocal of the macroscopic fast-neutron removal cross section, or the distance for an e-fold reduction in the fast-neutron flux. For the second, the travel is characterized by the Fermi age. For the third, the thermal-neutron diffusion area is used, but this is so small in most shield media that it can be ignored in comparison to the first two processes.

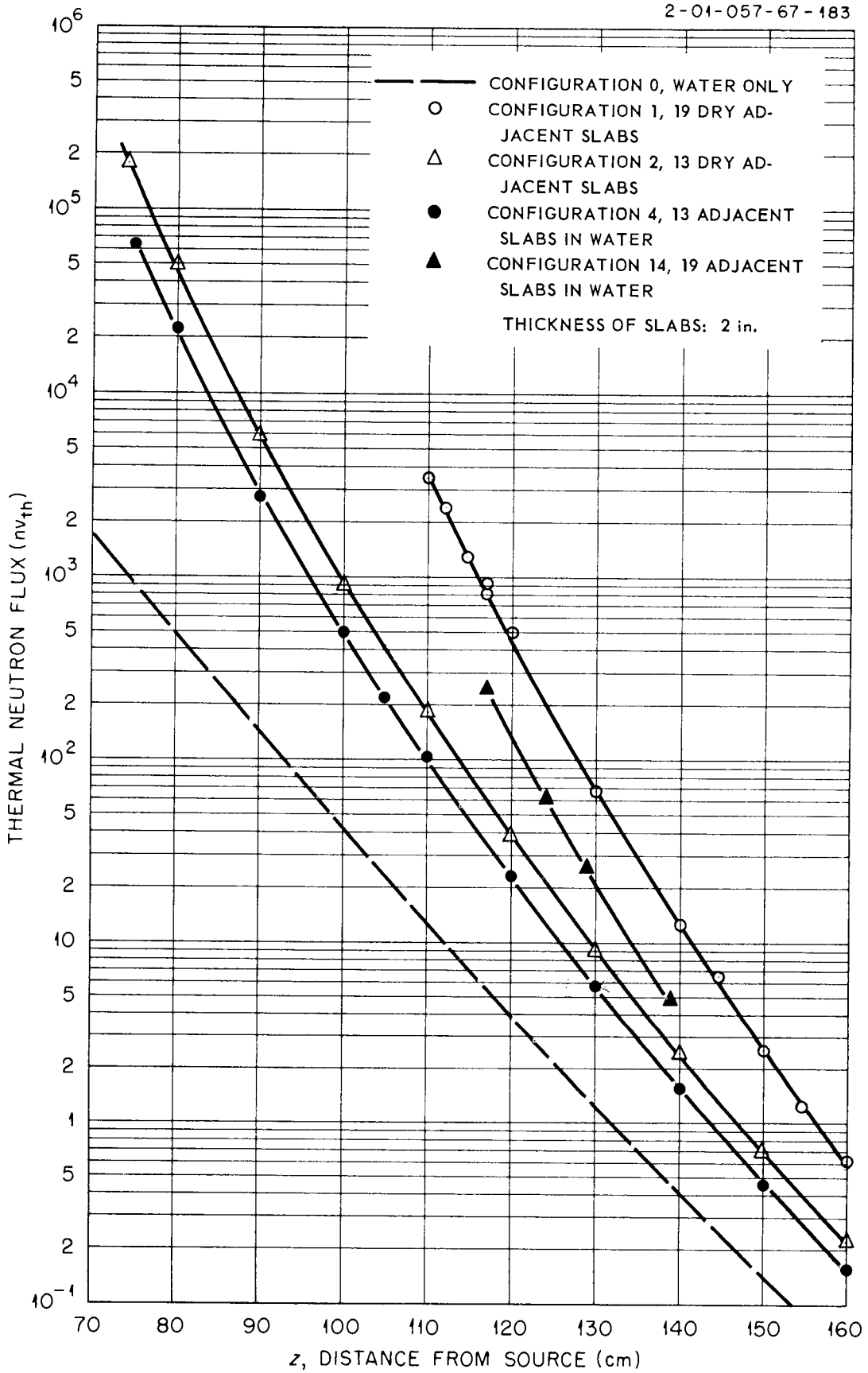

Fig. 2. Thermal-Neutron Flux in Water Beyond Configurations 1, 2, 4, and 14 as a Function of Distance from the Source: Comparison of the Attenuation of Adjacent Concrete Slabs in Air and Water Media.

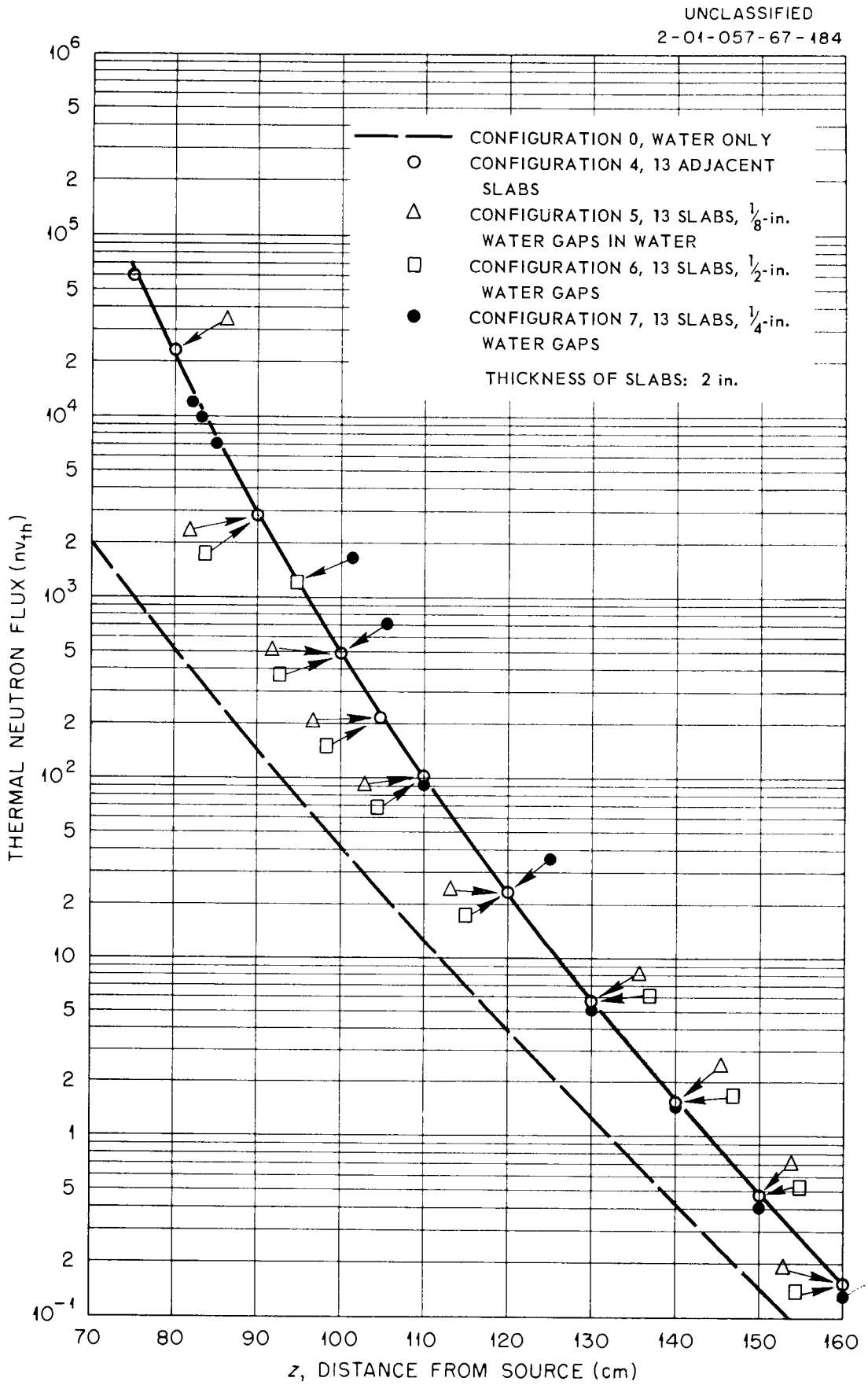

Fig. 3. Thermal-Neutron Flux in Water Beyond Configurations 4, 5, 6, and 7 as a Function of Distance from the Source: Effect of Introducing a $\frac{1}{8}$- to $\frac{1}{2}$-in.-thick Water Gap After Each 2-in. Thickness of Concrete.

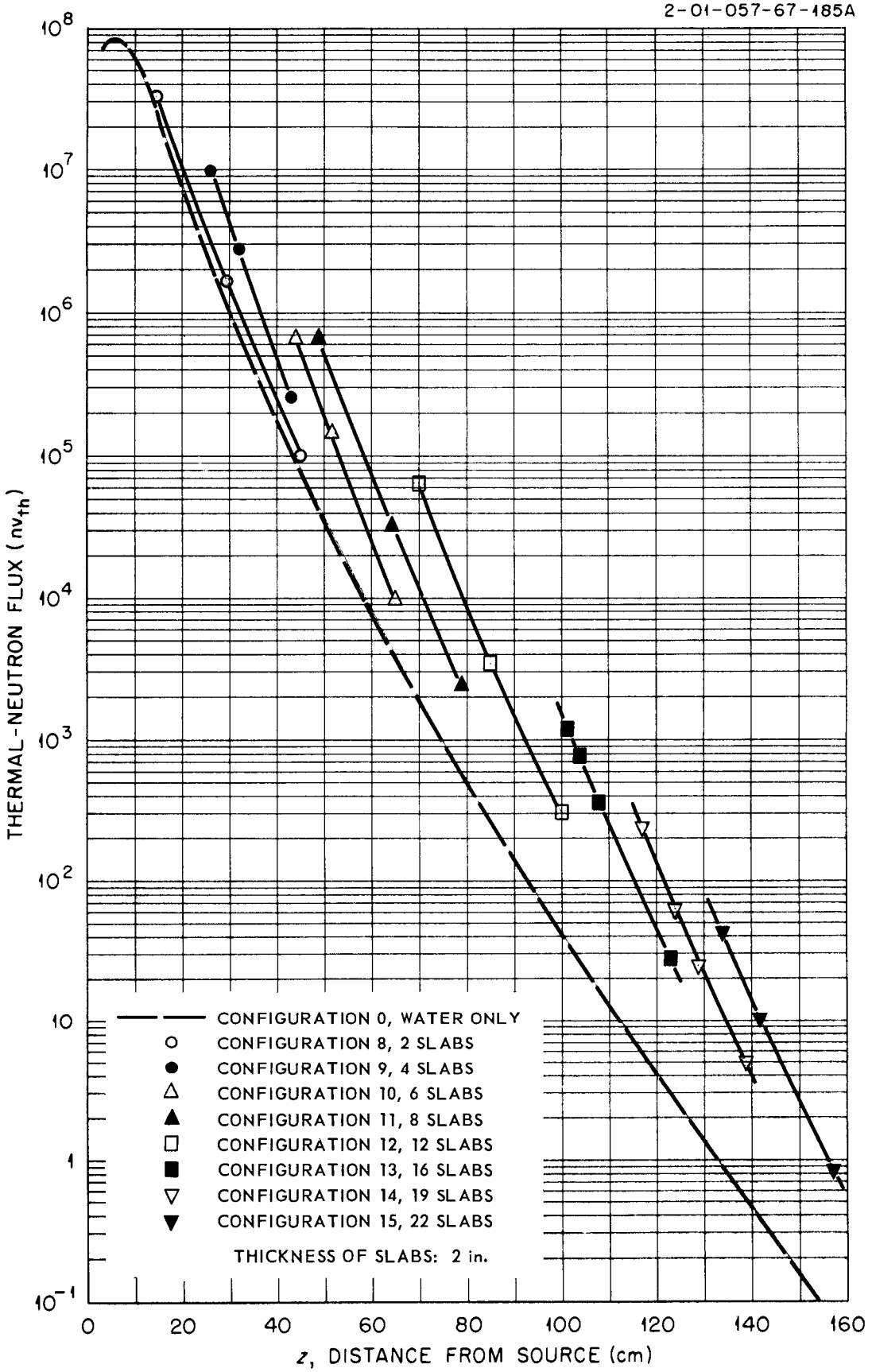

Fig. 4. Thermal-Neutron Flux in Water Beyond Configurations 8, 9, 10, 11, 12, 13, 14, and 15 as a Function of Distance from the Source: Effect of Increasing the Total Thickness of Adjacent Concrete Slabs in a Water Medium.

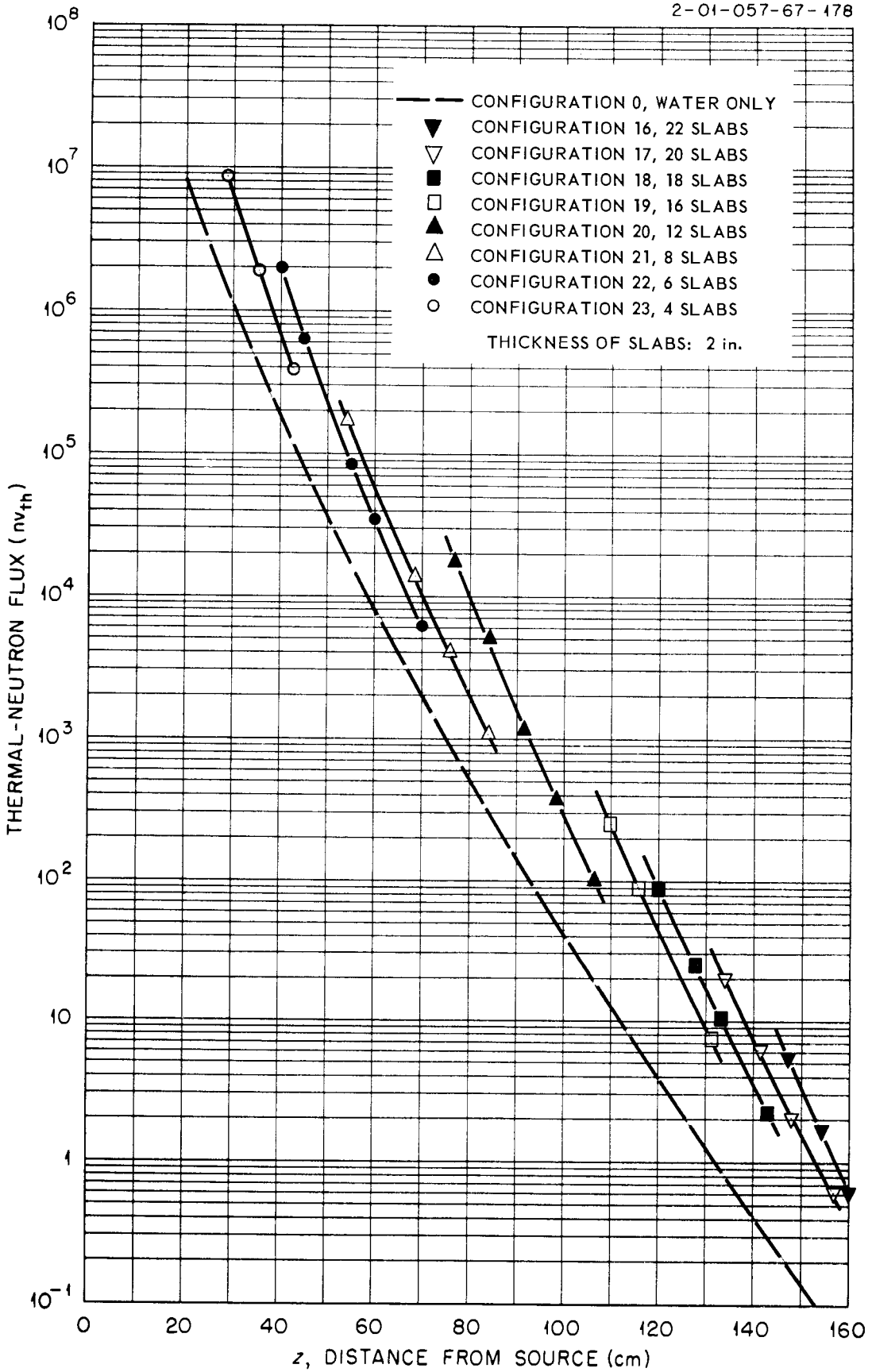

Fig. 5. Thermal-Neutron Flux in Water Beyond Configurations 16, 17, 18, 19, 20, 21, 22, and 23: Effect of Introducing a ½-in.-thick Water Gap After Each 4-in. Thickness of Concrete.

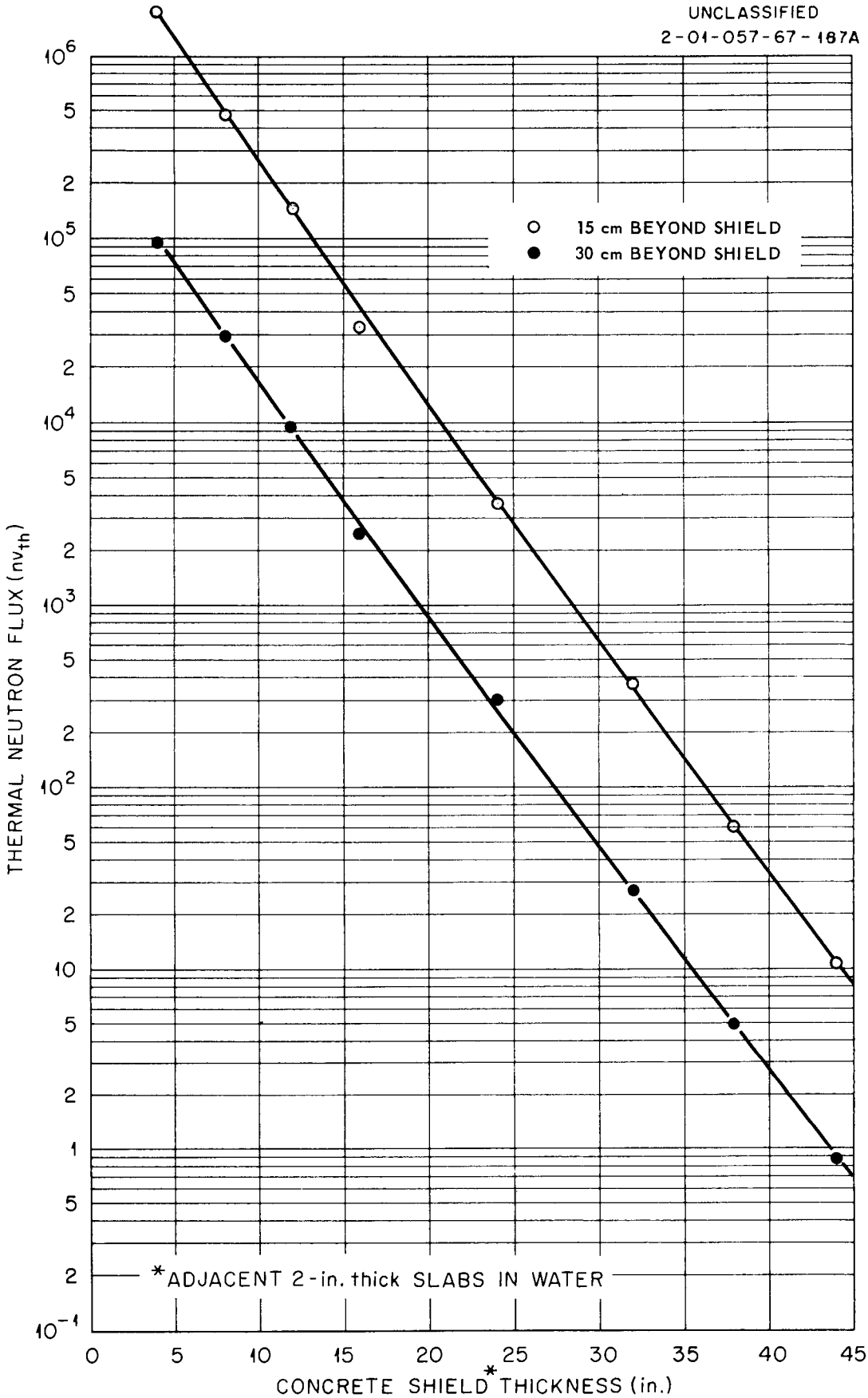

Fig. 6. Thermal-Neutron Flux in Water Beyond Various Thicknesses of a Concrete Shield in a Water Medium.

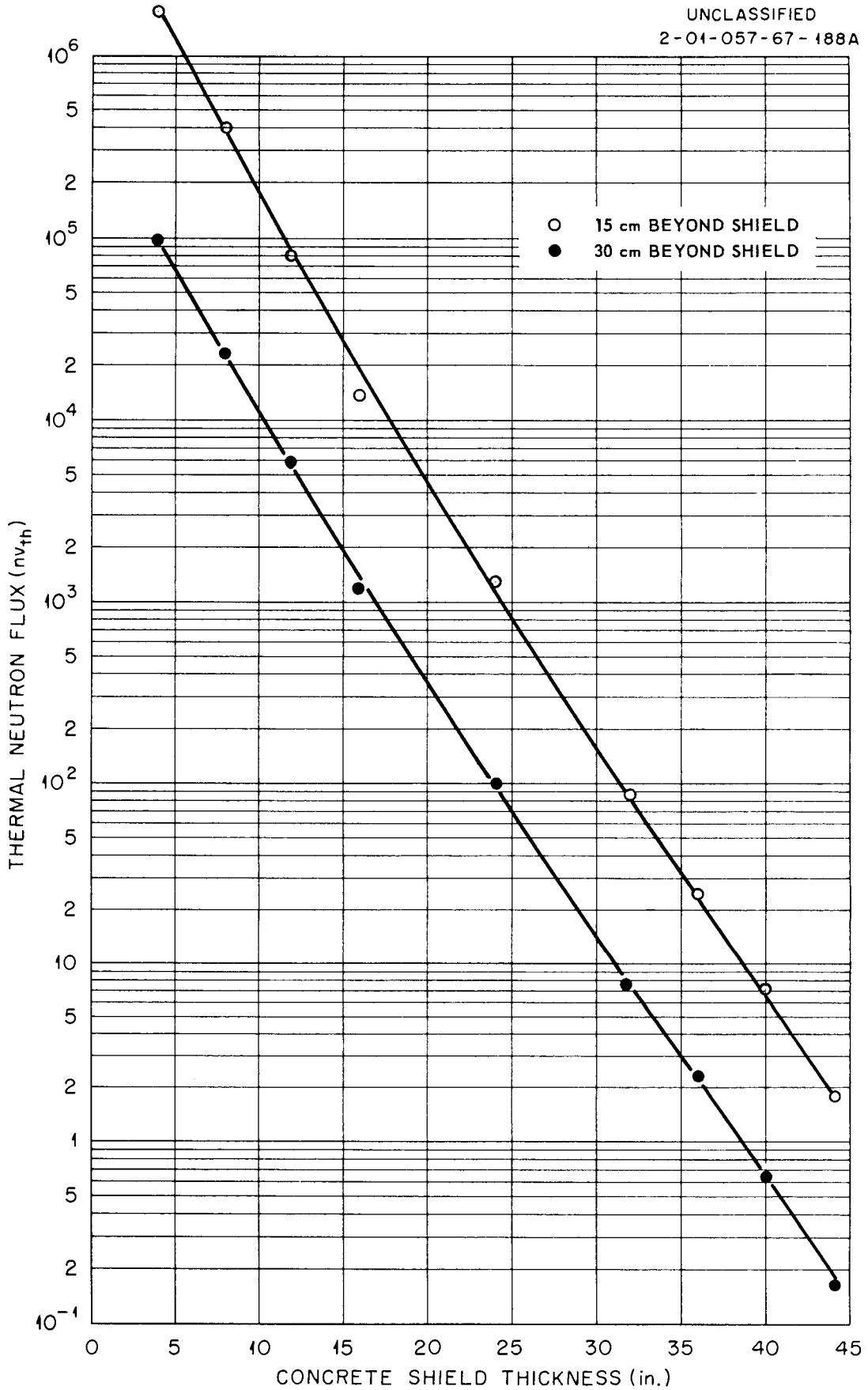

Fig. 7. Thermal-Neutron Flux in Water Beyond Various Thicknesses of a Concrete Shield in Which a ½-in.-thick Water Gap Follows Each 4-in. Thickness of Concrete.

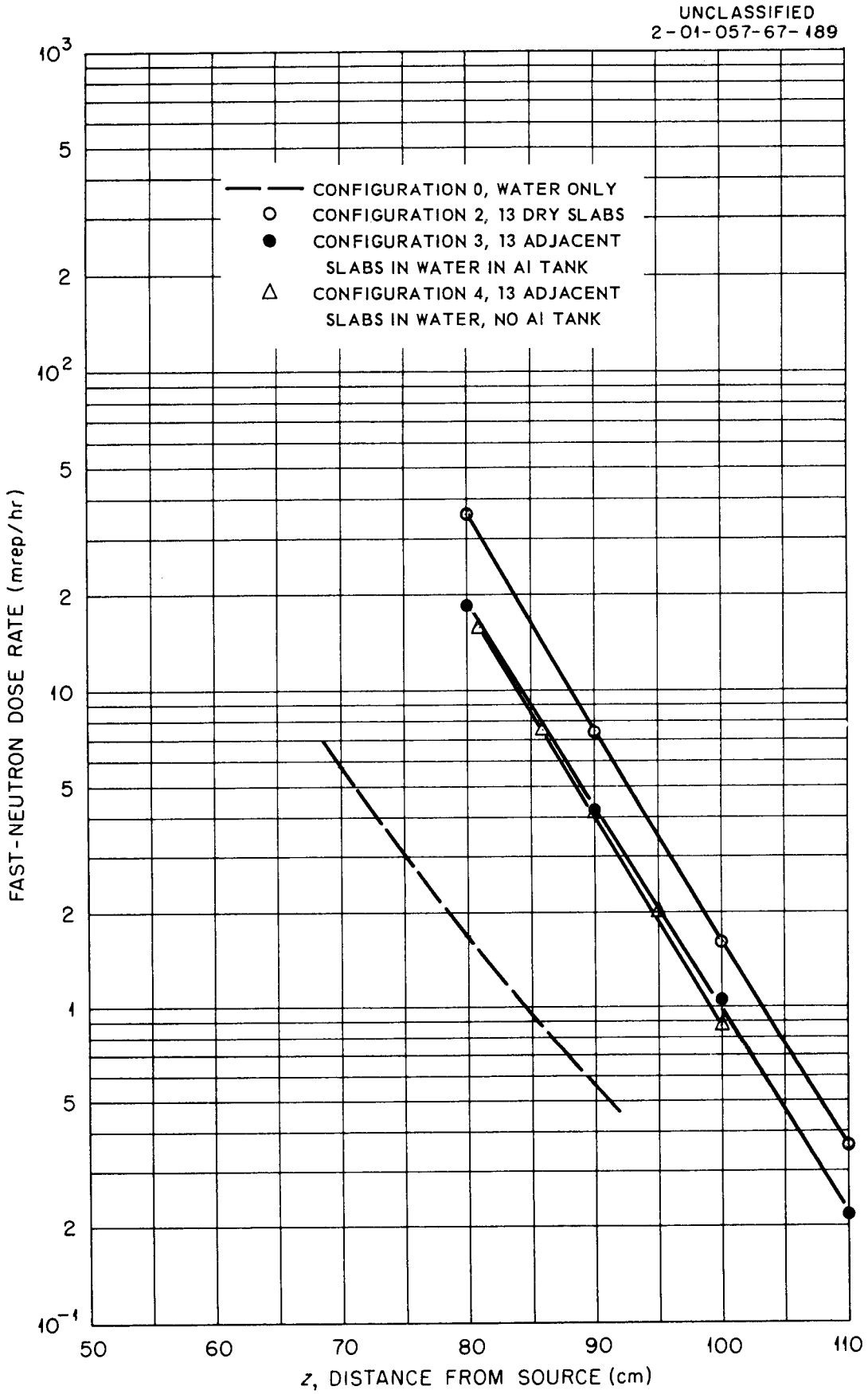

Fig. 8. Fast-Neutron Dose Rates in Water Beyond Configurations 2, 3, and 4 as a Function of Distance from the Source: Comparison of the Attenuation of Adjacent Concrete Slabs in Air and Water Media.

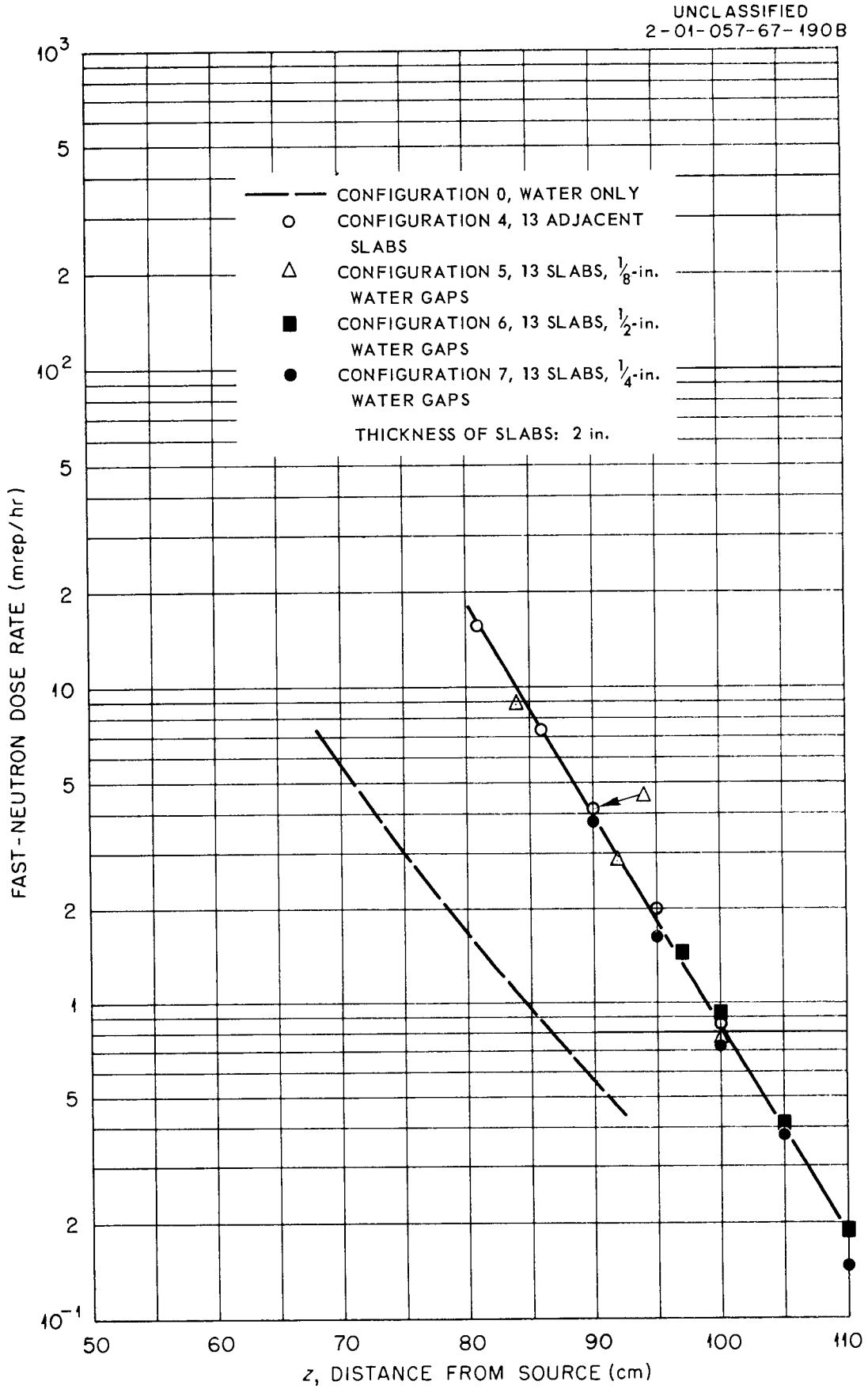

Fig. 9. Fast-Neutron Dose Rates in Water Beyond Configurations 4, 5, 6, and 7 as a Function of Distance from the Source: Effect of Introducing a 1/8- to 1/2-in.-thick Water Gap After Each 2-in. Thickness of Concrete.

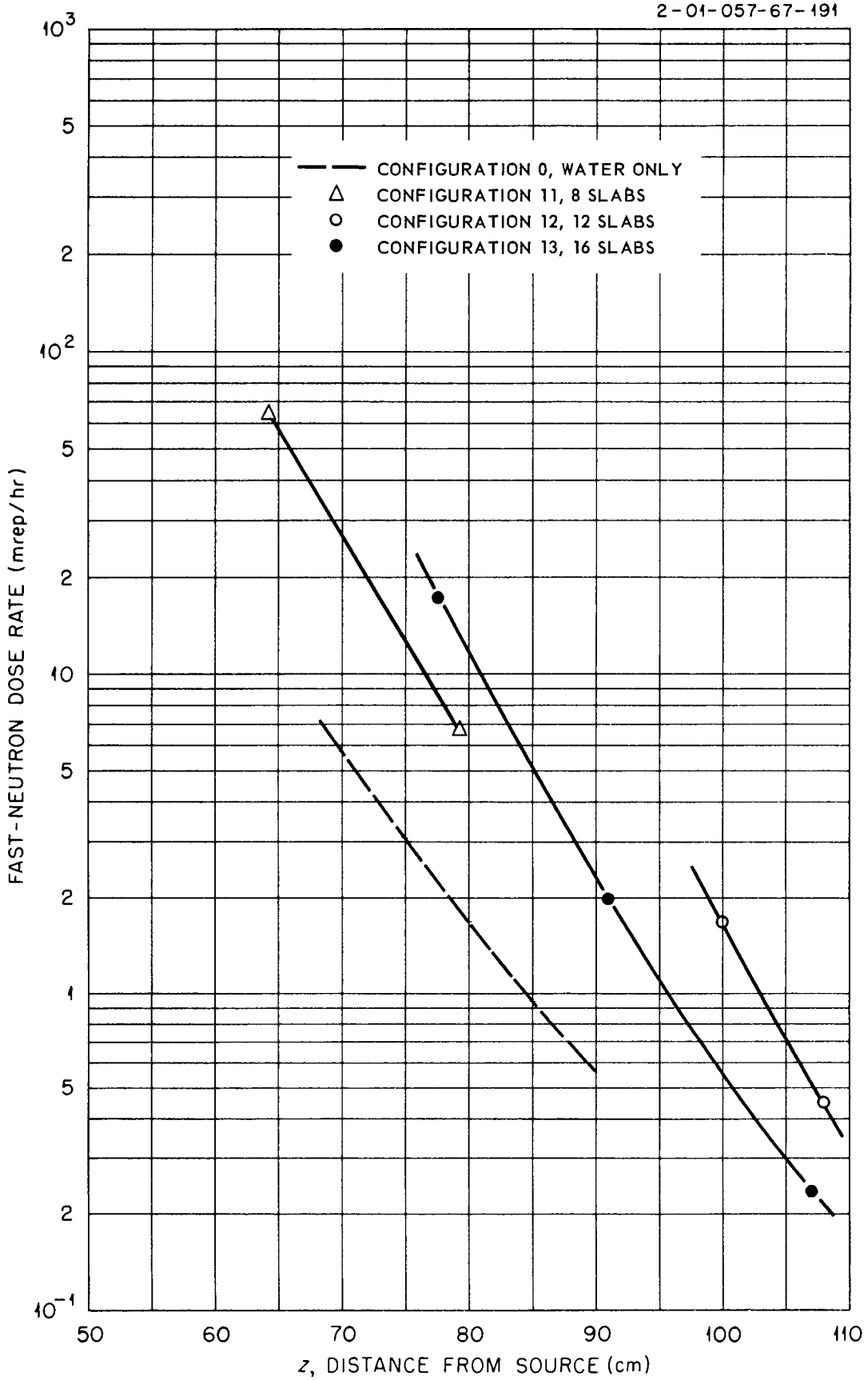

Fig. 10. Fast-Neutron Dose Rates in Water Beyond Configurations 11, 12, and 13 as a Function of Distance from the Source: Effect of Increasing the Total Thickness of Adjacent Concrete Slabs in a Water Medium.

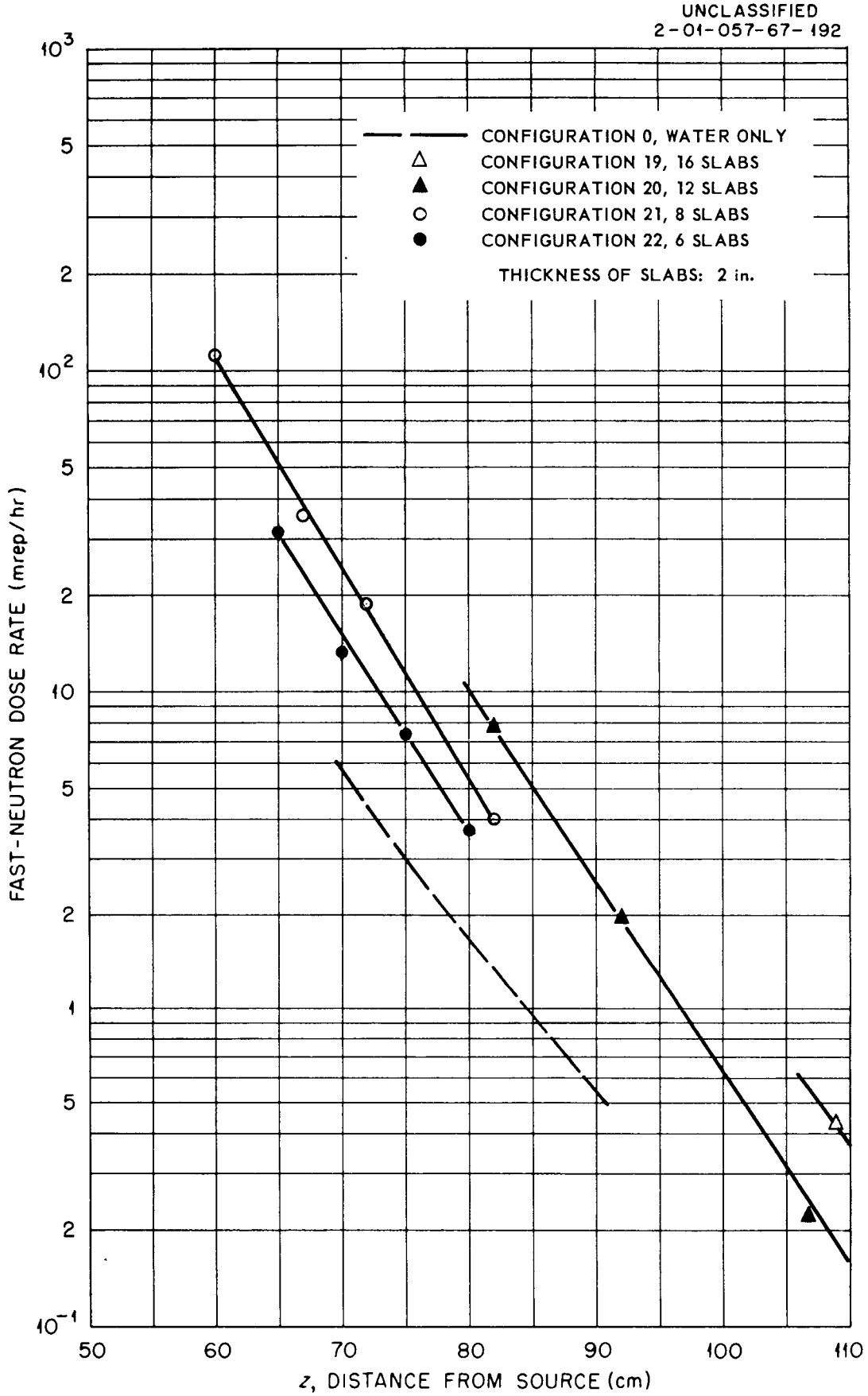

Fig. 11. Fast-Neutron Dose Rates in Water Beyond Configurations 19, 20, 21, and 22, as a Function of Distance from the Source Plate: Effect of Introducing a ½-in.-thick Water Gap After Each 4-in. Thickness of Concrete.

Overlaying these processes, the phenomenon of hardening of the neutron spectrum, due to the variation with energy of shield cross section, must be considered. This is a very strong effect in water, but is much less apparent in ordinary concrete, since in the latter case the cross sections do not vary so markedly for low and high energies (see Fig. 12).

Thus, the energy spectrum of neutrons in the shield will be characterized by several effects. At the inside, the fission source, peaking at 3/4 Mev, will be evident. Farther out, the very fast neutrons (3 to 8 Mev) will have penetrated largely without collision because of the lower cross section. The intermediate-energy component (epithermal to $\sim$1 Mev) will have originated partly in the fission source directly and partly in the collided faster neutrons. The attenuation of this slower component is of particular interest, since if it is less than that of the fast component, the moderation is less than adequate and can be improved by addition of water to the concrete. If, however, with the exception of a short initial transition region, the attenuation more or less matches the fast attenuation, then moderation is roughly adequate and the fast-neutron removal cross section concept will apply.

If water follows the concrete shield, the thermal-neutron flux distribution can be used to identify hard and intermediate-energy groups. The flux close to the concrete shows a short relaxation length in water and indicates the intermediate-energy group. (The thermal-neutron flux in water comes from faster neutrons slowing down in the immediate vicinity.) Farther out the harder neutrons will persist and the thermal-neutron flux there will indicate this component. In addition, dosimeter data will also indicate the hard group.

In order to determine the apparent attenuation of the intermediate-energy neutrons, the thermal-neutron flux measurements in water at 15 and at 30 cm beyond the concrete configurations of various thicknesses were examined. For "dry" configurations consisting of 19 and 13 slabs the fluxes at 15 cm were:

19 slabs (Conf. 1): $nv_{th} = 2.1 \times 10^2$ (from Fig. 2 at z = 123.9 cm)

13 slabs (Conf. 2): $nv_{th} = 7.6 \times 10^3$ (from Fig. 2 at z = 88.8 cm)

while the fluxes at 30 cm were:

19 slabs (Conf. 1): $nv_{th} = 1.45 \times 10^1$ (from Fig. 2 at z = 138.9 cm)

13 slabs (Conf. 2): $nv_{th} = 4.8 \times 10^2$ (from Fig. 2 at z = 103.8 cm)

UNCLASSIFIED
2-01-059-282

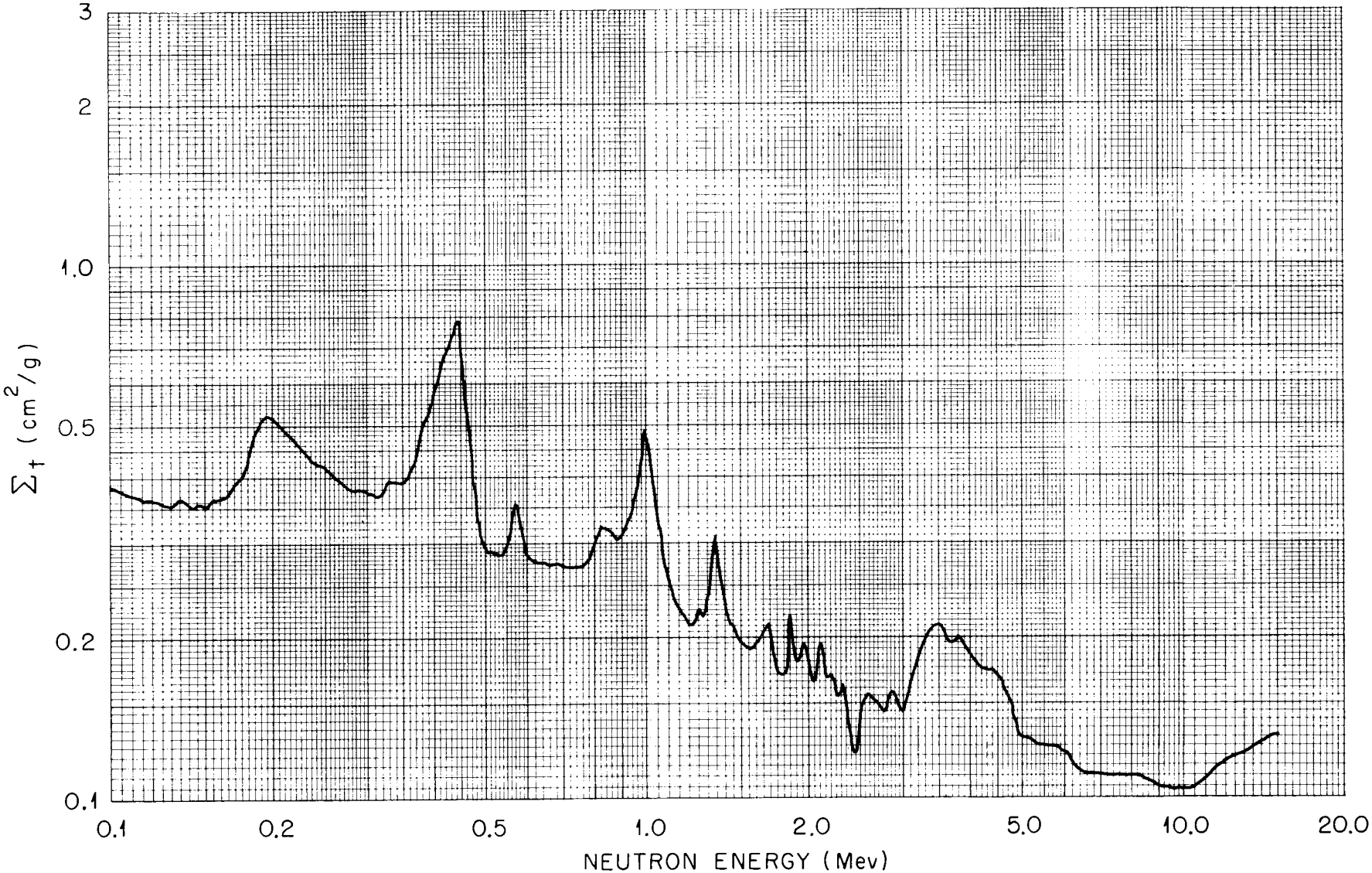

Fig. 12. Total Macroscopic Neutron Cross Sections for Portland Concrete.

In order to estimate the apparent attenuation of these intermediate-energy neutrons, the values at 15 and 30 cm in water behind the slabs are used to obtain a relaxation length which describes the additional attenuation of 19 slabs over that of 13 slabs. The geometric corrections required are essentially the same as those required for the removal cross-section determination, so that the following formula derived by Blizard and used by Chapman and Storrs[2] will apply:

$$\frac{D_{13}}{D_{19}} = \frac{\lambda_{13}}{\lambda_{19}}\left(\frac{t_{19}}{t_{13}}\right)^2 \left(1 - \frac{a^2 t_{19} - t_{13}}{4\lambda t_{13} t_{19} - a^2 t_{13}}\right) e^{\Sigma_R \Delta t}$$

where

D_{13}, D_{19} = thermal-neutron flux in the water beyond 13 or 19 slabs, respectively, at a distance of either 15 or 30 cm, here presumed to be be proportional to the intermediate-energy leakage flux, neutrons/cm^2·sec,

λ_{13}, λ_{19} = neutron relaxation lengths in water at points where D_{19} are measured (it is assumed here that $\lambda_{13} = \lambda_{19}$)

λ = average relaxation length, here taken to be about $(\Sigma_R)^{-1}$,

t_{13}, t_{19} = distances from source to points where D_{13} and D_{19} are measured,

Δt = difference in actual concrete thickness (normal) between the 19- and 13-slab configuration,

Σ_R = macroscopic removal cross section for this energy neutron component; the value of Σ_R is here used to mean that, for a point source in an infinite medium, the dose will be described by a function of the form $e^{-\Sigma_R R}/R^2$, where R is the distance from the source to the detector.

Σ_R is assumed to be only a slowly varying function of R, the values of which are obtained from the data as follows:

For 15 cm of H_2O: $\Sigma_R = 0.101\ cm^{-1}$, $\lambda = 9.9$ cm

For 30 cm of H_2O: $\Sigma_R = 0.101\ cm^{-1}$, $\lambda = 9.9$ cm

The foregoing values are for intermediate-energy neutrons. Fast neutrons can be observed by noting fluxes at greater distances in water beyond the concrete. By comparison of data from the 13-slab dry configuration with the pure water data, it is possible to obtain a fast-neutron removal cross section by an identical method. The result, using data 76.2 cm beyond the concrete, was:

$$\Sigma_R(\text{meas., fast}) = 0.087\ cm^{-1};\ \lambda(\text{meas., fast}) = 11.5\ cm$$

From removal cross sections reported by Chapman and Storrs,[7] which describe the attenuation of very energetic neutrons, the values are (see Table 5)

$$\Sigma_R(\text{calc.}) = 0.089\ cm^{-1};\ \lambda_R = 11.3\ cm,$$

Table 5. Calculation of Fast-Neutron Removal Attenuation Coefficient for Dry Ordinary Concrete

Element	Concentration (wt%)	Σ_R/ρ (cm^2/g)[a]	wt%$\cdot\Sigma_R/\rho$ (cm^2/g)
O	46.7	3.72×10^{-2}	1.74×10^{-2}
S	0.29	2.77×10^{-2}	0.01×10^{-2}
Si	14.3	3.01×10^{-2}	0.43×10^{-2}
Fe	1.10	2.14×10^{-2}	0.02×10^{-2}
Al	3.54	2.92×10^{-2}	0.10×10^{-2}
P	0.31	2.83×10^{-2}	0.01×10^{-2}
Mn	0.11	2.02×10^{-2}	0
C	4.92	4.07×10^{-2}	0.20×10^{-2}
H	0.83	5.98×10^{-2}	0.50×10^{-2}
Na	0.45	3.41×10^{-2}	0.02×10^{-2}
K	0.18	2.47×10^{-2}	0
Ca	24.32	2.43×10^{-2}	0.59×10^{-2}
Mg	2.40	3.33×10^{-2}	0.08×10^{-2}
		TOTAL	3.70×10^{-2}

a. Values of the neutron removal cross section, Σ_R, are taken from ORNL-1843, G. T. Chapman and C. L. Storrs, "Effective Neutron Removal Cross Sections for Shielding," (Aug. 1955).

7. ORNL-1843, op. cit.

which is in good agreement with this measurement. Thus the intermediate-energy neutrons are being attenuated more strongly than the very fast neutrons, indicating adequate moderation within the concrete. The shield attenuation rate then will be characteristic of the very fast neutrons and described by the removal cross-section calculation. It is to be remembered that this conclusion applies to "dry" slabs, i.e., with 7.48 wt% water.

The addition of water to insure that the attenuation of intermediate-energy neutrons at least matches that of the fast neutrons is very desirable. It might also be desirable, in order further to reduce the dose at the outside, to add more water to reduce the magnitude of the intermediate-energy flux which accompanies the fast flux. The criterion for this is that the dose from intermediate-energy neutrons should not constitute a major fraction of the whole dose. Unfortunately, it is not easy to determine very precisely the intermediate-energy dose, but an estimate can be obtained from a simple correction formula between fast- (in this case intermediate-energy) neutron current and thermal-neutron flux:[8]

$$I_{fast}(z) = \lambda \Sigma_a \phi_{th}(z) e^{-\tau/\lambda^2}$$

where

$I_{fast}(z)$ = fast-neutron current in the water at z,

$\phi_{th}(z)$ = thermal-neutron flux at z,

Σ_a = thermal-neutron absorption cross section in water = 0.02 cm^{-1},

τ = age from fast to thermal energy of neutrons in water cm^2,

λ = average relaxation length for thermal-neutron flux in water, cm.

The foregoing formula can be used quite well for the intermediate-energy neutrons.

---

8. E. P. Blizard, "Introduction to Shield Design," ORNL-CF-51-10-70 (Jan., 1952).

By extrapolation to the back of the last slab, the flux at the outside of the 19-slab dry configuration is found to be 4.6×10^3 n/cm^2/sec and $\lambda = 4.8$ cm. It is necessary to estimate some mean effective "fast" neutron energy at this region, and this is done from the relaxation length λ, assuming λ is of the order of magnitude of the mean free path in hydrogen:

$$\Sigma_H = \frac{1}{4.8}$$

$$\sigma_H = \frac{18}{(2)(4.8)(0.602 \times 10^{24})} \text{ cm}^2 = 3.12 \text{ barns}$$

From this, it is found that the effective energy is about 1.7 Mev.

The value of τ is that determined by Coveyou,[9] $\tau \approx 22$ cm^2. Thus,

$$I_{fast} = (4.8)(0.02)(4.6 \times 10^3)\, e^{-22/(4.8)^2}$$

$$= 1.7 \times 10^2 \text{ neutrons/cm}^2\cdot\text{sec}$$

Since 57 neutrons/cm^2·sec of energy 1.7 Mev gives 0.3 rem per 40-hr week,[10] or, using RBE = 10, 0.75 mrep/hr,

$$76 \text{ neutrons/cm}^2\cdot\text{sec} \sim 1 \text{ mrep/hr}$$

$$I_{fast} \sim 170/76 \text{ mrep/hr}$$

$$\cong 2.2 \text{ mrep/hr}$$

There is no comparable measurement with a fast-neutron dosimeter for this point, but such a measurement is available for comparison for 12- and 13-slab configurations. These are given in the following Table 6.

Table 6. Comparison of Fast-Neutron Dosimeter Measurements with Fast-Neutron Dose Determinations from Thermal-Neutron Flux Measurements Beyond Concrete Samples

Configuration		Fast-Neutron Dose at Back of Last Slabs (mrep/hr)	
No.	Description	Calculated from Thermal-Neutron Flux	Measured with Dosimeter
2	13 2-in.-thick slabs, dry	76	96
7	13 2-in.-thick slabs with 1/4-in.-thick water gaps between them	7.2	16
20	12 2-in.-thick slabs with 1/2-in.-thick water gaps following every second slab	9.4	18

9. R. R. Coveyou, "Calculated Ages of Monoenergetic Neutrons in Mixtures of Light and Heavy Water," (to be published).

10. "Protection Against Neutron Radiation up to 30 Million Electron Volts," National Bureau of Standards Handbook 63, p. 62.

There is no comparable measurement for 19 slabs with the fast-neutron dosimeter, but data are available for 13 slabs dry, 13 slabs with added water, and 12 slabs with added water. The doses for these cases have been calculated from thermal-neutron fluxes as in the example above and are compared in Table 6 with the dosimeter data.

It will be seen that the dosimeter reading is higher in every case, but of the same order of magnitude. The higher reading may be attributed either to uncertainties in the calculation or to the effect of the fastest neutron component, which would be marked by the lower energy one in the thermal-neutron measurements near the last concrete slab. The second entry in Table 6 gives data for concrete with more water* and shows a resulting strong reduction in dose. Similarly, in Figs. 3 and 9 the data are shown for several different water thicknesses in the concrete, indicating in every case that the water added <u>in</u> the concrete is very nearly of the same effectiveness as water following the shield. If there were a very sharp spectrum change associated with increased water content, the several curves in water following the concrete would be of different shape. Since no great difference is evident, the water content of the "dry" slabs must be adequate, and the water is acting principally as a fast-neutron attenuator. Its effect is well described by the effective removal cross-section concept.

---

*In this experiment additional water content in the concrete is approximated by the inclusion of water layers, or gaps, between slabs. Since these are small and closely spaced, the approximation should be good, but to insure that this is the case other experiments were made in which the approach to homogeneity was less. Thus, in Configuration 20 the gaps were 1/2 in. every 4 in., which is to be compared to Configuration 7 in which the gaps are 1/4 in. thick every 2 in. These two cases give quite comparable results, indicating little effect attributable to nonhomogeneity.

Gamma-Ray Attenuation

The attenuation of concrete for gamma rays was not in as unsettled a state as that of neutrons, but during the course of the experiment gamma-ray dose-rate measurements were made beyond the various configurations, and, in order to show that the present calculational method does fit the data, a check calculation was made. The experimental data are shown in Figs. 13 through 20. The calculation was performed to determine the dose rate at the rear of configuration 1, in which there were 19 dry slabs of concrete (96.5 cm of concrete). The sources that were considered were

(1) prompt fission gamma rays,

(2) gamma rays produced by neutron capture in the uranium of the source plate, and

(3) gamma rays produced by neutron capture in the concrete.

The spectrum of gamma rays produced in coincidence with fission was taken from the work of Gamble.[11] The gamma-ray attenuation coefficients for the several elements in concrete came from White,[12] and buildup factors were taken from the calculations of Goldstein and Wilkins.[13] Geometric corrections, based on exponential attenuations, to take care of the finite size of the source plate were taken from the paper of Welton and Blizard.[14]

The spectra were divided into five energy groups: 0 - 1 Mev, 1 - 3 Mev, 3 - 5 Mev, 5 - 7 Mev, and >7 Mev. (The group for photons of energy >7 Mev were assigned an energy of 8 Mev.) The attenuation for each group was calculated, the contributions then being added.

---

11. Roger Gamble, PhD. thesis, "Prompt Fission Gamma Rays from U^{235}," Univ. of Texas, June, 1955.

12. Gladys R. White, "X-ray Attenuation Coefficients from 10 kev to 100 Mev," NBS-1003 (May, 1952).

13. Herbert Goldstein and J. Ernest Wilkins, Jr., "Calculations of the Penetration of Gamma Rays," NYO-3075 (June 30, 1954).

14. T. A. Welton and E. P. Blizard, Reactor Science and Technology TID-2002, Vol. 2, No. 2 (August, 1952) (Classified).

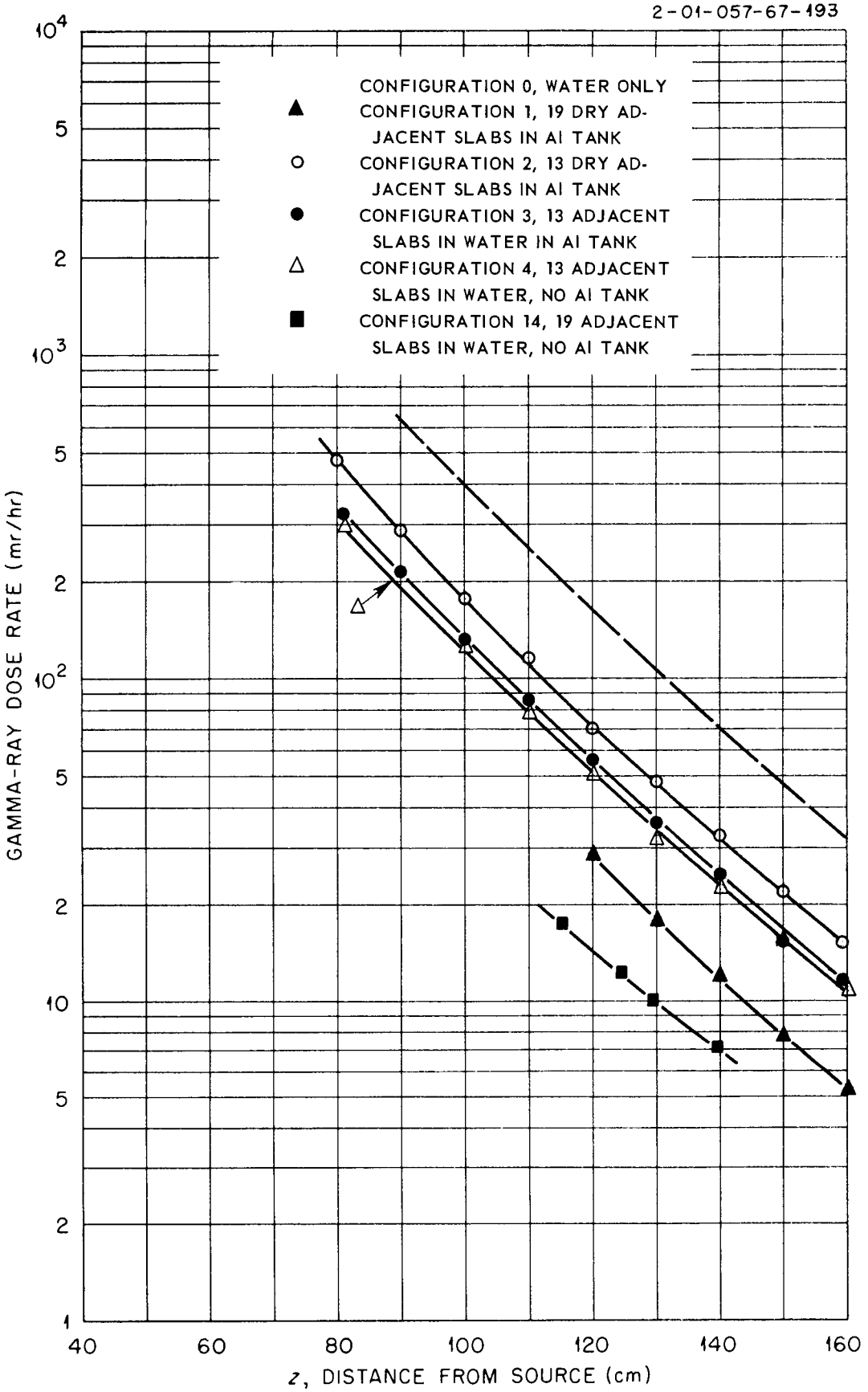

Fig. 13. Gamma-Ray Dose Rates in Water Beyond Configurations 1, 2, 3, 4, and 14 as a Function of Distance from the Source: Comparison of the Attenuation of Adjacent Concrete Slabs in Air and Water Media.

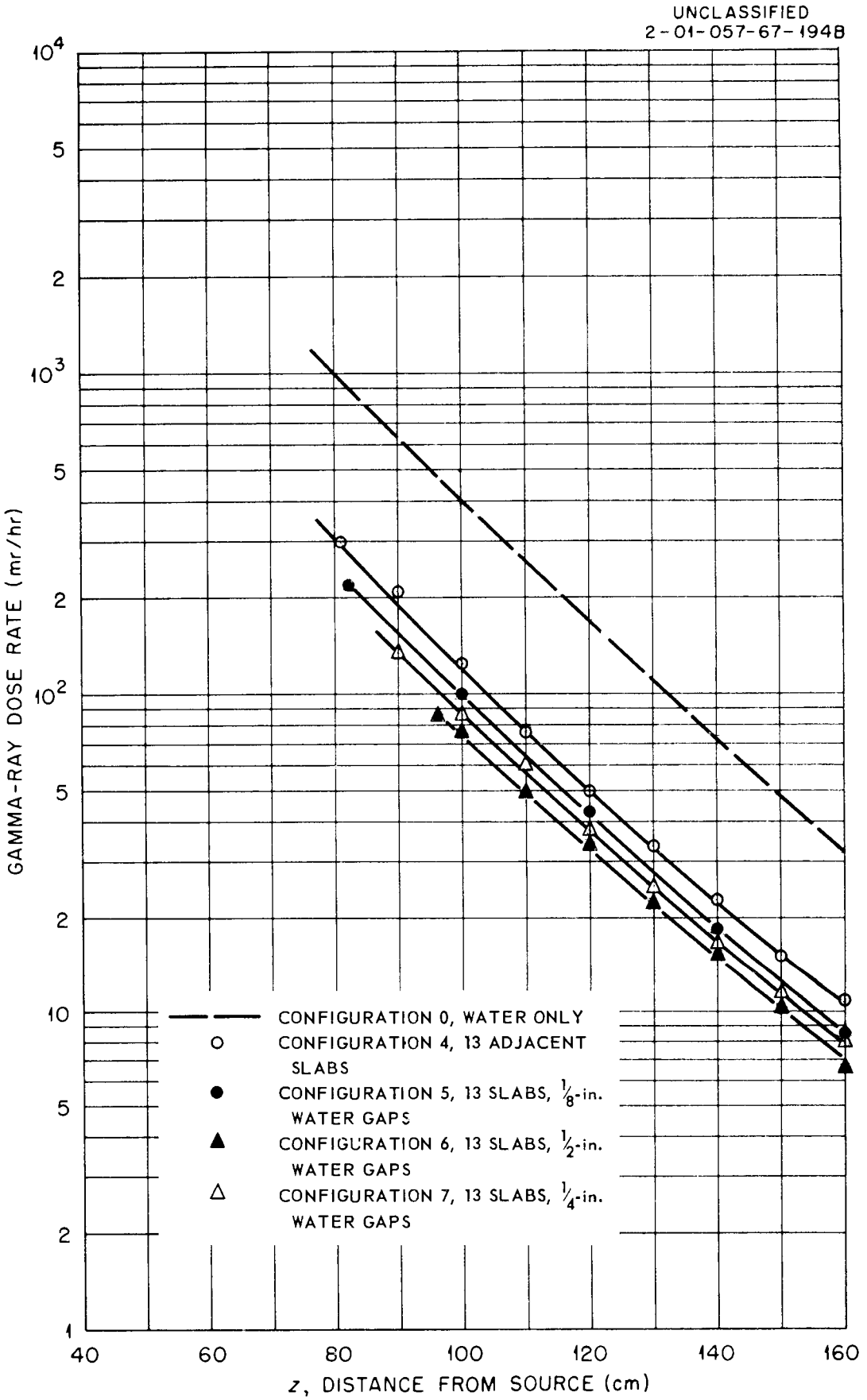

Fig. 14. Gamma-Ray Dose Rates in Water Beyond Configurations 4, 5, 6, and 7 as a Function of Distance from the Source: Effect of Introducing a 1/8- to 1/2-in.-thick Water Gap After Each 2-in. Thickness of Concrete.

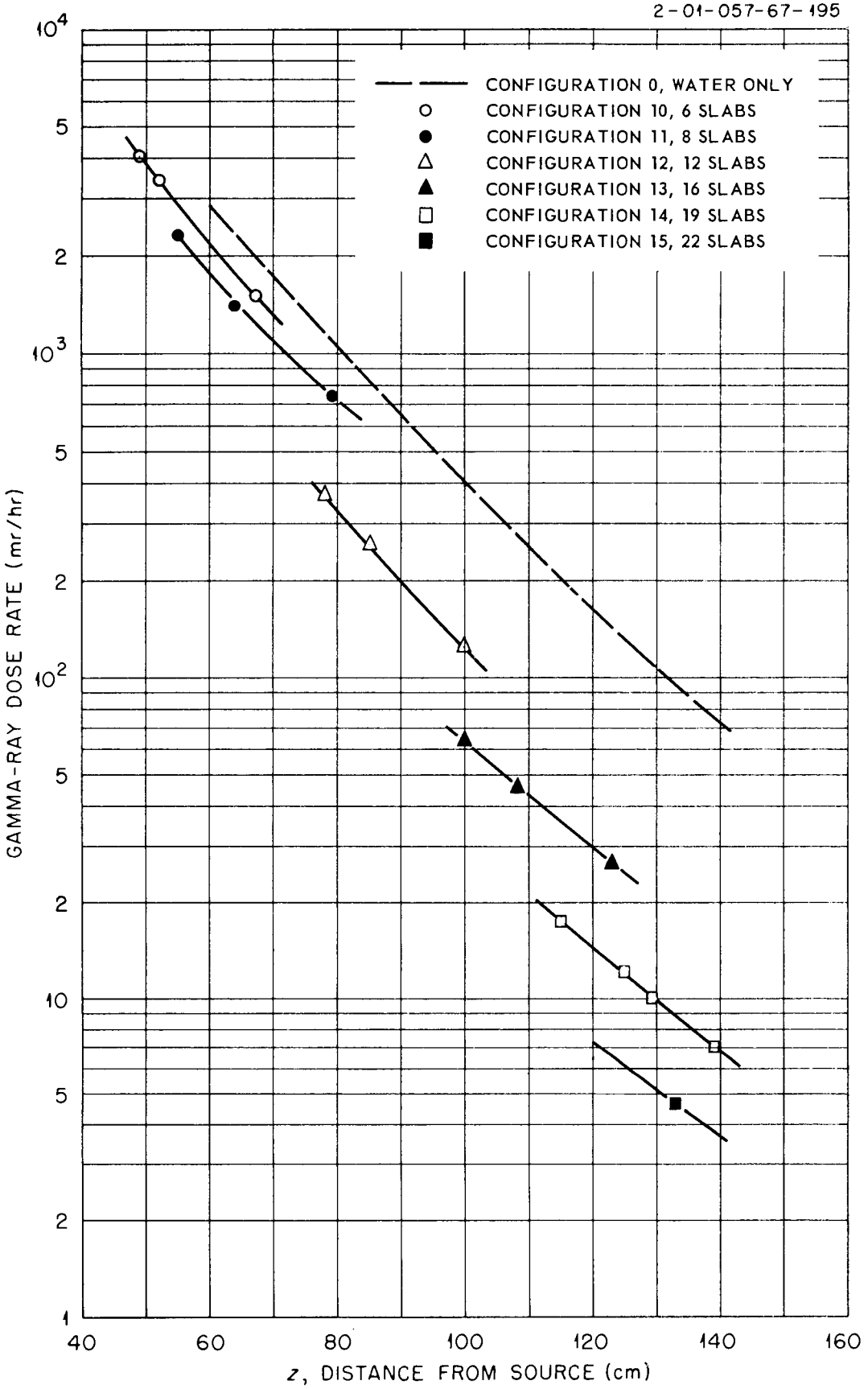

Fig. 15. Gamma-Ray Dose Rates in Water Beyond Configurations 10, 11, 12, 13, 14, and 15 as a Function of Distance from the Source: Effect of Increasing the Total Thickness of Adjacent Concrete Slabs in a Water Medium.

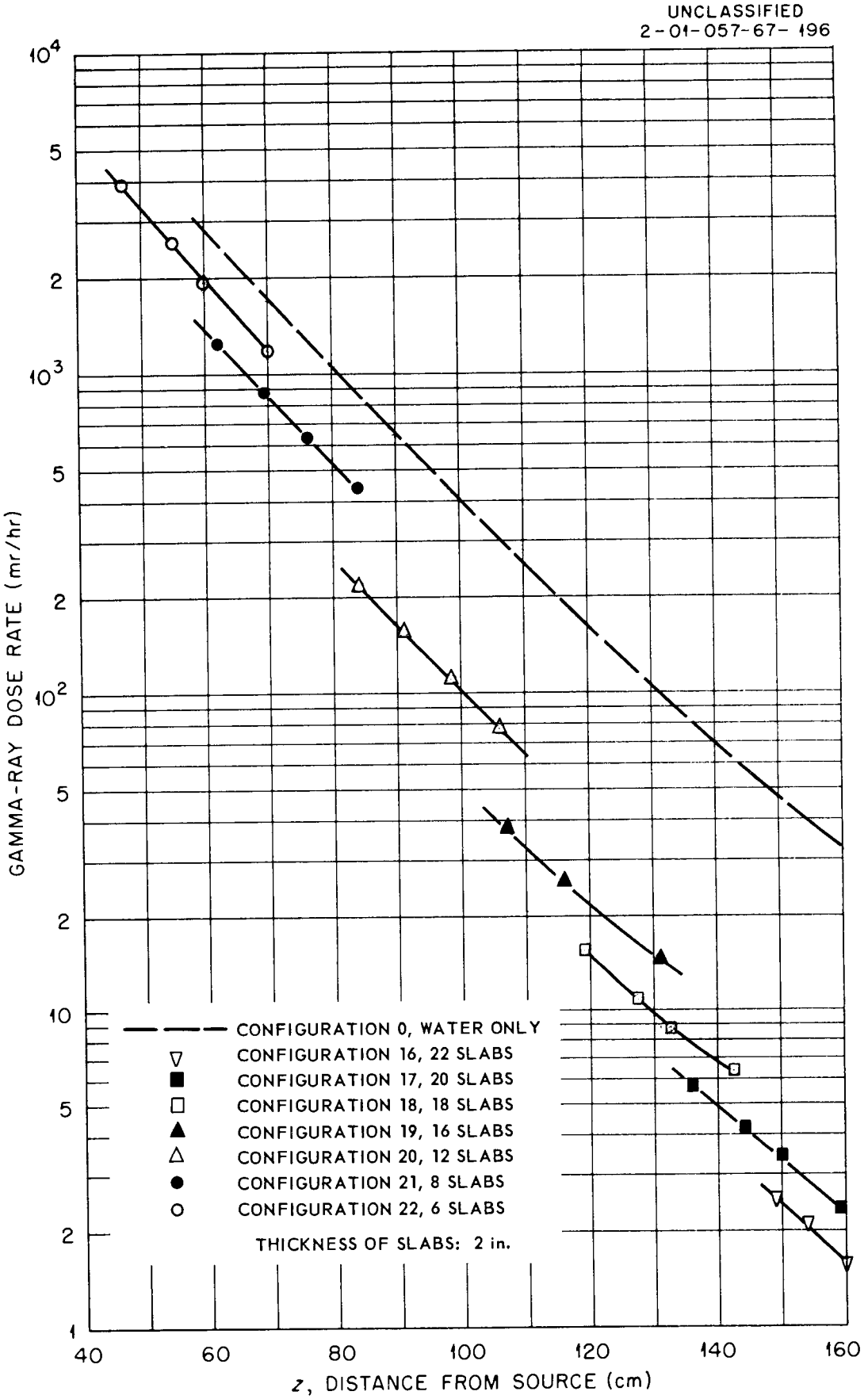

Fig. 16. Gamma-Ray Dose Rates Beyond Configurations 16, 17, 18, 19, 20, 21, and 22 as a Function of Distance from the Source: Effect of Introducing a ½-in.-thick Water Gap After Each 4-in. Thickness of Concrete.

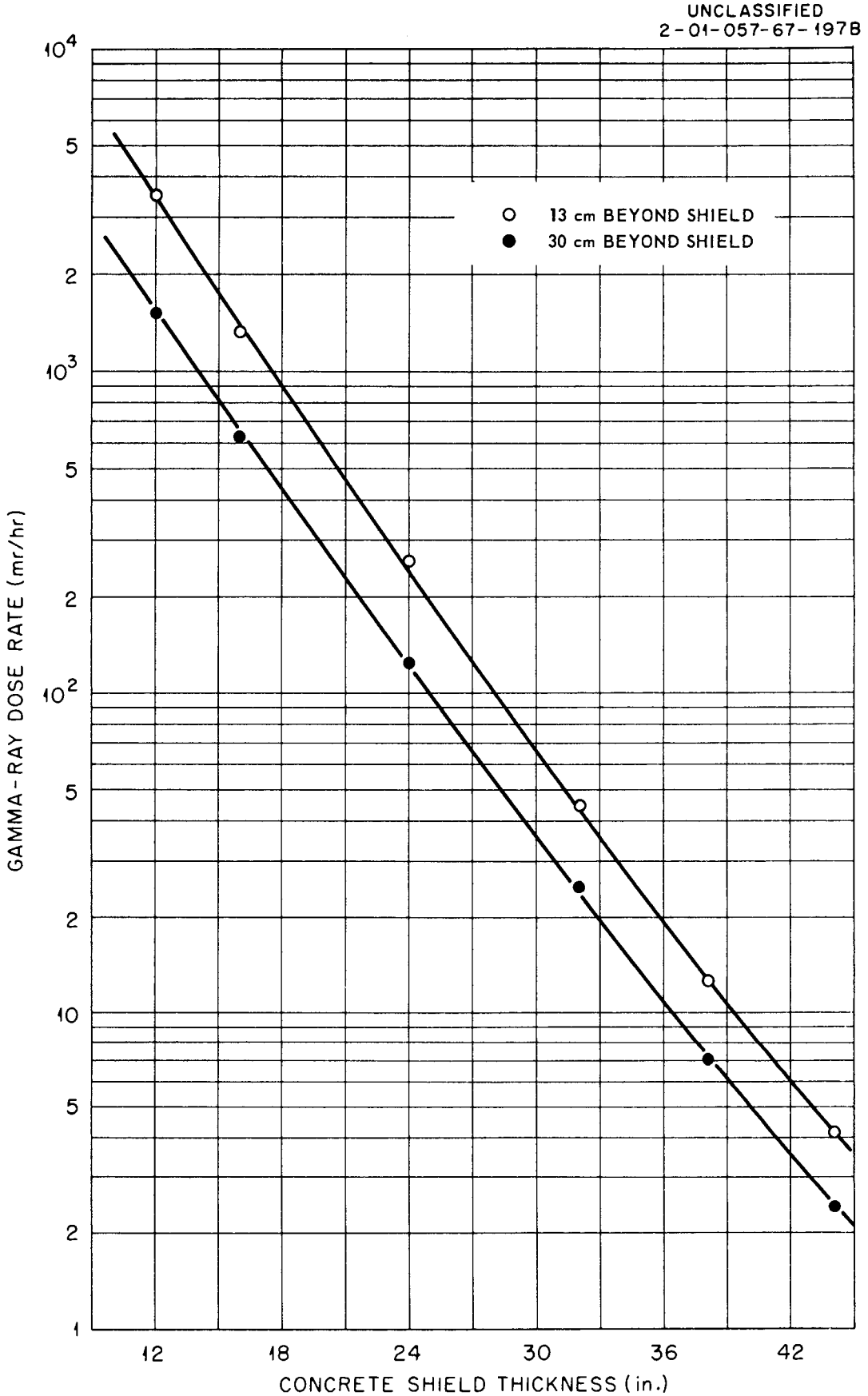

Fig. 17. Gamma-Ray Dose Rates in Water Beyond Various Thicknesses (in inches)* of a Concrete Shield. *Plotted in centimeters in Fig. 19.

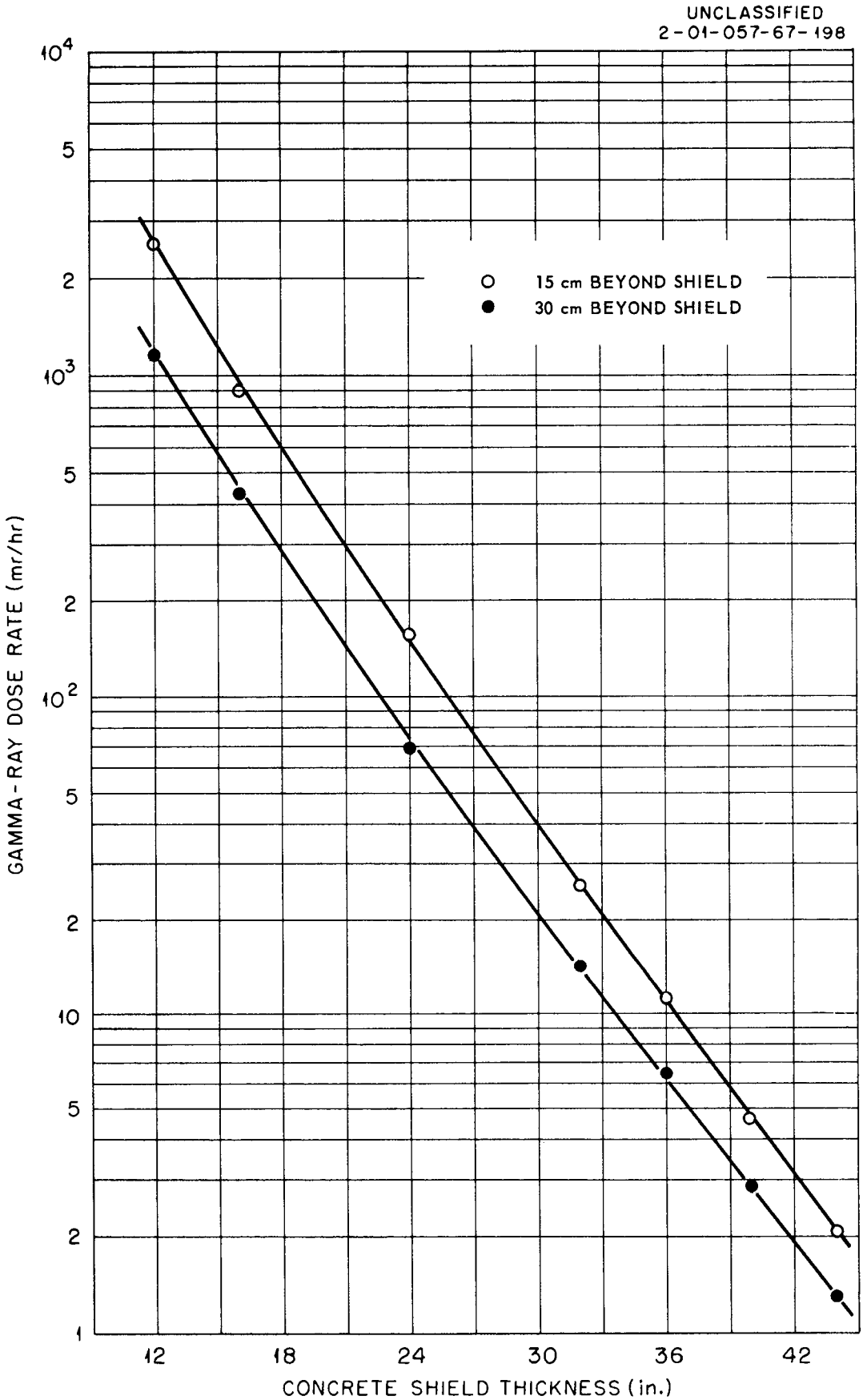

Fig. 18. Gamma-Ray Dose Rates in Water Beyond Various Thicknesses (in inches)* of a Concrete Shield in Which a ½-in.-thick Water Gap Follows Each 4-in. Thickness of Concrete. *Plotted in centimeters in Fig. 20.

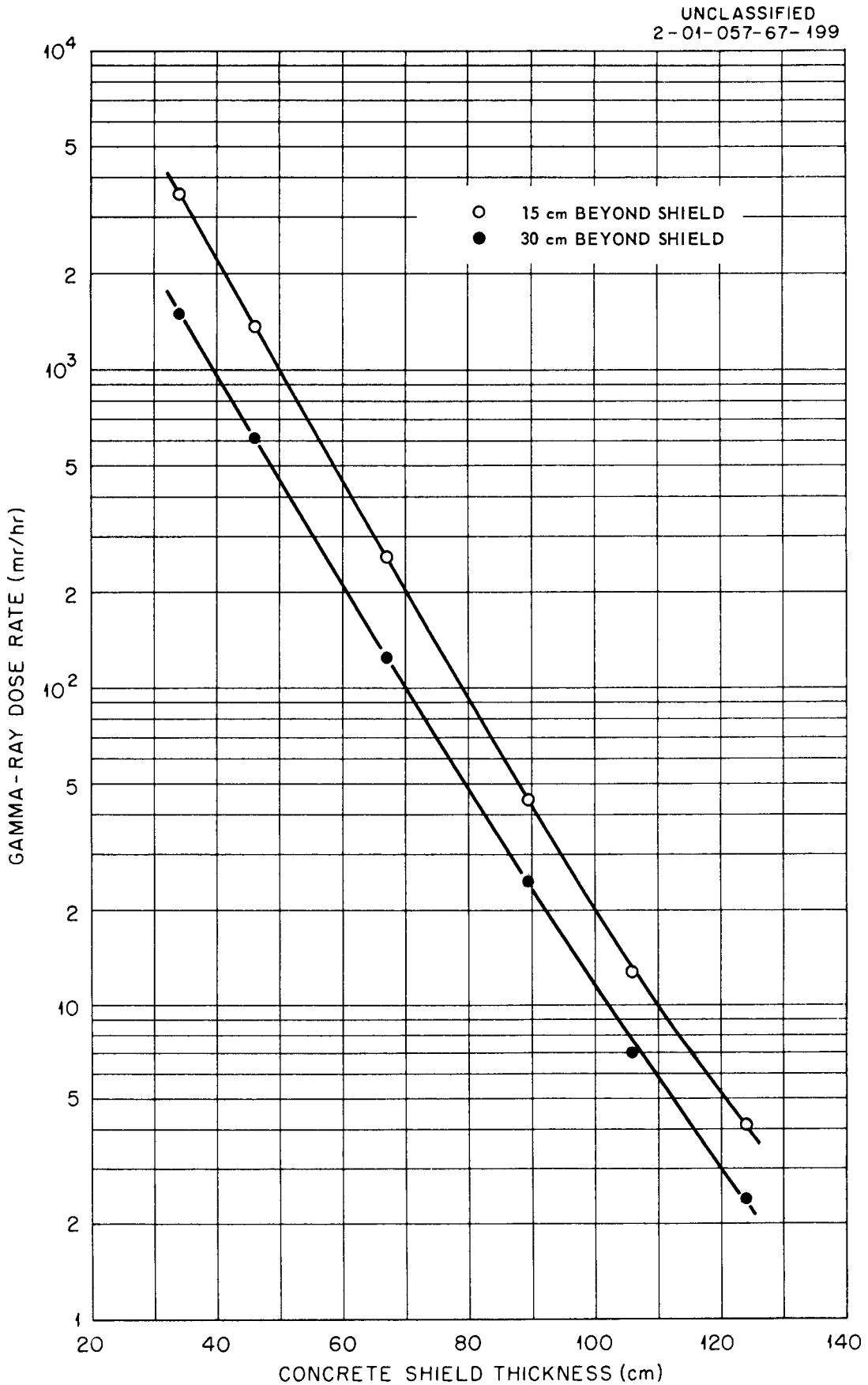

Fig. 19. Gamma-Ray Dose Rates in Water Beyond Various Thicknesses (in centimeters)* of a Concrete Shield. *Plotted in inches in Fig. 17.

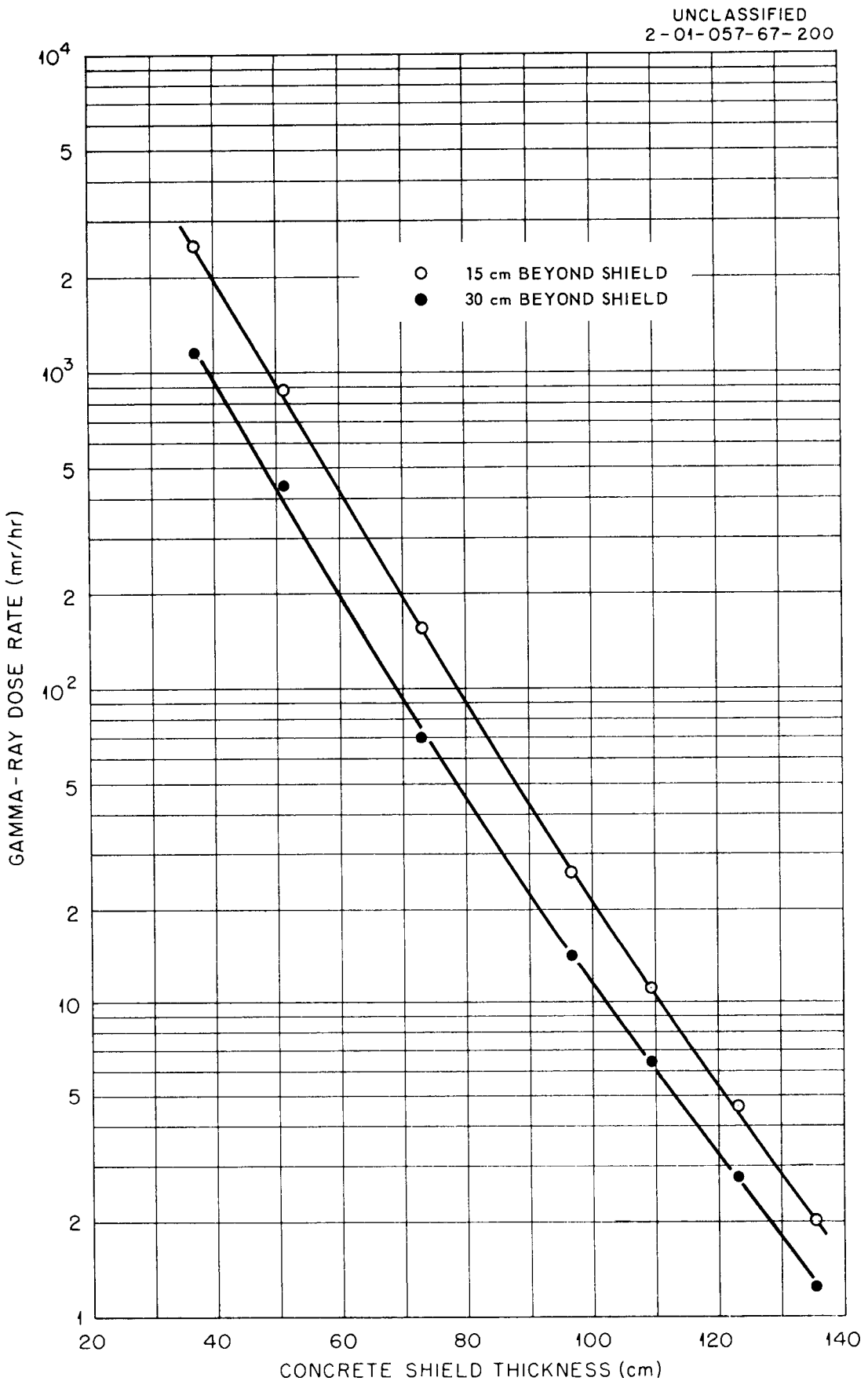

Fig. 20. Gamma-Ray Dose Rates in Water Beyond Various Thicknesses (in centimeters)* of a Concrete Shield in Which a ½-in.-thick Water Gap Follows Each 4-in. Thickness of Concrete. *Plotted in inches in Fig. 18.

Using the foregoing, the dose, in reps/hr, resulting from prompt fission gamma rays is given by:

$$D_p = C\left(\frac{F}{\pi a^2}\right)(P_iE_i)\left(\frac{\mu_a}{\rho}\right)_{i,air} B(\mu_i z)\left(\frac{e^{-\mu_i z}}{4\pi z^2}\right)\left(\frac{2\pi z}{\mu_i}\right)\left(1 - e^{-\mu_i a^2/2z}\, e^{-\mu_{iU} t}\right)$$

where

i = subscript denoting photon energy group,

C = factor to convert from photon energy flux times attenuation coefficient for air to reps/hr

= 5.767×10^5 reps/hr,

F = fission rate in source,

= 5.32×10^{10} fissions/sec,

a = radius of source plate

= 35.6 cm,

P_iE_i = source spectrum from Gamble's data[11] multiplied by photon energy (photons per energy interval times the energy interval times the mean energy in the interval),

$\left(\frac{\mu_a}{\rho}\right)_{i,air}$ = mass attenuation coefficient for air for photons of the ith energy interval (cm^2/g),

$B(\mu_i z)$ = buildup factor for the ith energy interval and z cm of concrete, μ_i being the linear attenuation coefficient of concrete (cm^{-1}) (buildup factors for aluminum were actually used since it is a low-Z element, much like the components of concrete),

$e^{-\mu_i z}/4\pi z^2$ = attenuation kernel for uncollided flux,

$\frac{2\pi z}{\mu_i}\left(1 - e^{-\mu_i a^2/2z}\right)$ = geometric correction for finite source disk size,

$e^{-\mu_{iU} t}$ = attenuation in uranium source plate, t being taken as equal to the radius of the uranium fuel cylinders which comprised the source (see Section I).

The results of the calculation for each energy interval are shown in Table 7.

Table 7. Calculated Gamma-Ray Dose Rates Beyond Configuration 1

Energy Range (Mev)	Source Strength (photons/sec)	Attenuation Coefficient (cm^{-1})	Dose Rate (mrep/hr)
	From Prompt Fission Gamma Rays		
0 - 1	1.37×10^{11}	0.211	0.00005
1 - 3	1.93×10^{11}	0.106	0.22
3 - 5	5.15×10^{10}	0.076	0.5
5 - 7	1.45×10^{10}	0.0647	0.2
7 (8)	1.19×10^{9}	0.060	0.02
			0.9
	From Uranium Capture Gamma Rays		
4	1.17×10^{10}	0.0761	5.5
	From Concrete Capture Gamma Rays		
0 - 1	9.4×10^{8}	0.21	5.5×10^{-4}
1 - 3	4.35×10^{10}	0.106	5.61×10^{-1}
3 - 5	3.46×10^{10}	0.076	3.69×10^{0}
5 - 7	2.88×10^{10}	0.0647	7.65×10^{0}
7 (8)	5.62×10^{9}	0.060	2.36×10^{0}
			14.3
Total			21

The calculation for the dose, D_U, resulting from gamma rays produced by neutron capture in uranium was then carried out in a similar manner, although it was required for only one energy. It was presumed that 18% of the absorptions of U^{235} of the fission plate were nonfission absorptions giving capture gamma rays. Lacking experimental information, it was assumed that each capture gave one 4-Mev gamma ray, others being of low enough energy to be ignored. The results of this calculation are also given in Table 7.

A calculation to determine the dose, D_c, resulting from gamma rays produced by neutron capture in concrete was required for each energy interval, since fast neutrons from the source plate are slowed down in the concrete and captured, giving rise to gamma rays of various energies. It was presumed that the slowing down was gaussian, with a Fermi age, τ, of 103 cm^2 (Ref. 15). If the attenuation of gamma rays thence is approximately exponential with a relaxation length λ, the effect of the distributed source can be estimated by assuming that the neutrons are captured at a distance into the concrete equal to τ/λ (Ref. 16). In this calculation different "displacement distances," τ/λ_i, were used according to the values of λ for the several energies. Neutron attenuation in the source and its housing was taken as 0.6. The results again are given in Table 7.

It can be seen from Table 7 that the total calculated gamma-ray dose rate is 21 mrep/hr. The measured gamma-ray dose rate in the water following configuration 1 was extrapolated to the back of the last slab with a resulting dose rate of 46 $\pm$ 10 mrep/hr. The agreement between the calculated and measured values is as good as can be expected on the basis of information which was used. The indication is that the buildup factors for aluminum as calculated by Goldstein and Wilkins apply reasonably well to concrete.

---

15. R. R. Coveyou, "Age of Fission Neutrons in Concretes," (to be published).

16. "Materials Testing Reactor Project Handbook," TID-7001, p. 187 (May 7, 1951).

Appendix A

TABULATION OF THE RADIATION MEASUREMENTS BEYOND THE CONFIGURATIONS

z, Distance from Source (cm)	Thermal-Neutron Flux (nv_{th})	Fast-Neutron Dose Rate (mrep/hr)	Gamma-Ray Dose Rate (mr/hr)
	Plain Water		
4	7.6×10^{7}		
6	8.49×10^{7}		
10	5.92×10^{7}		
20	8.21×10^{6}		
30	1.16×10^{6}		
40	1.73×10^{5}		
50	3.51×10^{4}		
60	8.04×10^{3}		2.85×10^{3}
70	1.95×10^{3}	5.78×10^{0}	1.70×10^{3}
80	5.32×10^{2}	1.70×10^{0}	1.05×10^{3}
90	1.42×10^{2}	5.59×10^{-1}	6.38×10^{2}
100	4.10×10^{1}		4.02×10^{2}
110	1.24×10^{1}		2.56×10^{2}
120	3.96×10^{0}		1.66×10^{2}
130	1.26×10^{0}		1.12×10^{2}
140	4.33×10^{-1}		7.17×10^{1}
150	1.50×10^{-1}		4.69×10^{1}
160	4.87×10^{-2}		3.20×10^{1}
	Configuration 1		
110	3.43×10^{3}		
112	2.33×10^{3}		
115	1.23×10^{3}		
117	7.79×10^{2}		
	9.18×10^{2}		
120	4.99×10^{2}		2.78×10^{1}
130	6.72×10^{1}		1.78×10^{1}

z, Distance from Source (cm)	Thermal-Neutron Flux (nv_{th})	Fast-Neutron Dose Rate (mrep/hr)	Gamma-Ray Dose Rate (mr/hr)
	Configuration 1 (cont'd.)		
140	1.25×10^{1}		1.19×10^{1}
145	5.48×10^{0}		
150	2.54×10^{0}		7.80×10^{0}
155	1.22×10^{0}		
160	6.14×10^{-1}		5.36×10^{0}
	Configuration 2		
74	1.77×10^{5}		
80	5.10×10^{4}	3.57×10^{1}	4.67×10^{2}
84			
90	5.80×10^{3}	6.95×10^{0}	2.85×10^{2}
		7.53×10^{0}	
100	9.01×10^{2}	1.59×10^{0}	1.76×10^{2}
110	1.75×10^{2}	3.60×10^{-1}	1.13×10^{2}
120	3.75×10^{1}		7.06×10^{1}
130	9.07×10^{0}		4.76×10^{1}
140	2.38×10^{0}		3.24×10^{1}
150	6.90×10^{-1}		2.14×10^{1}
159			1.55×10^{1}
160	2.12×10^{-1}		
	Configuration 3		
80		1.89×10^{1}	
81			3.17×10^{2}
90		4.11×10^{0}	2.12×10^{2}
100		1.04×10^{0}	1.32×10^{2}
105			
110			8.50×10^{1}
120			5.49×10^{1}
130			3.54×10^{1}
140			2.46×10^{1}
			1.60×10^{1}
159			1.18×10^{1}

z, Distance from Source (cm)	Thermal-Neutron Flux (nv_{th})	Fast-Neutron Dose-Rate (mrep/hr)	Gamma-Ray Dose Rate (mr/hr)
	Configuration 4		
75	6.16×10^{4}		
80	2.34×10^{4}		
81		1.57×10^{1}	2.98×10^{2}
86		7.40×10^{0}	
90	2.84×10^{3}	4.14×10^{0}	2.08×10^{2}
95		1.99×10^{0}	
100	4.96×10^{2}	8.41×10^{-1}	1.22×10^{2}
105	2.16×10^{2}		
110	1.02×10^{2}		7.64×10^{1}
120	2.29×10^{1}		5.09×10^{1}
130	5.79×10^{0}		3.34×10^{1}
140	1.58×10^{0}		2.23×10^{1}
150	4.64×10^{-1}		1.52×10^{1}
160	1.54×10^{-1}		1.08×10^{1}
	Configuration 5		
80	2.24×10^{4}		
82			2.15×10^{2}
84		8.93×10^{0}	
90	2.91×10^{3}	4.05×10^{0}	
92		2.87×10^{0}	
100	4.69×10^{2}	7.98×10^{-1}	1.00×10^{2}
105	2.08×10^{2}		
110	1.01×10^{2}		
120	2.29×10^{1}		4.28×10^{1} 3.87×10^{1}
130	5.63×10^{0}		
140	1.50×10^{0}		1.89×10^{1}
150	4.45×10^{-1}		
160	1.41×10^{-1}		8.68×10^{0}

z, Distance from Source (cm)	Thermal-Neutron Flux (nv_{th})	Fast-Neutron Dose-Rate (mrep/hr)	Gamma-Ray Dose-Rate (mr/hr)
	Configuration 6		
90	2.50×10^{3}		
95	1.20×10^{3}		
96			8.79×10^{-1}
97		1.47×10^{0}	
100	4.81×10^{2}	9.28×10^{-1}	7.71×10^{1}
105	2.12×10^{2}	4.05×10^{-1}	
110	9.57×10^{1}	1.88×10^{-1}	4.99×10^{1}
120	2.10×10^{1}		3.22×10^{1}
130	5.28×10^{0}		2.26×10^{1}
140	1.44×10^{0}		1.54×10^{1}
150	4.31×10^{-1}		1.06×10^{1}
160	1.24×10^{-1}		7.17×10^{0}
	Configuration 7		
82	1.20×10^{4}		
83	9.98×10^{3}		
85	7.07×10^{3}		
90	2.71×10^{3}	3.82×10^{0}	1.38×10^{2}
95	1.09×10^{3}	1.61×10^{0}	
100	4.55×10^{2}	7.21×10^{-1}	8.79×10^{1}
105		3.76×10^{-1}	
110	8.83×10^{1}	1.44×10^{-1}	6.01×10^{1}
120	1.97×10^{1}		3.74×10^{1}
130	4.91×10^{0}		2.43×10^{1}
140	1.37×10^{0}		1.66×10^{1}
150	3.91×10^{-1}		1.14×10^{1}
160	1.24×10^{-1}		6.55×10^{0}

z, Distance from Source (cm)	Thermal-Neutron Flux (nv_{th})	Fast-Neutron Dose Rate (mrep/hr)	Gamma-Ray Dose-Rate (mr/hr)
	Configuration 8		
15.3	3.10×10^{7}		
29.6	1.76×10^{6}		
44.6	9.86×10^{4}		
	Configuration 9		
26.4	9.86×10^{6}		
32.4	2.78×10^{6}		
43.5	2.52×10^{5}		
	Configuration 10		
44	7.60×10^{5}		
49			3.99×10^{3}
52.1	1.46×10^{5}		3.37×10^{3}
67.1	9.64×10^{3}		1.50×10^{3}
	Configuration 11		
49	6.81×10^{5}		
55			2.28×10^{3}
64.1	3.23×10^{4}	6.38×10^{1}	1.38×10^{3}
79.1	2.43×10^{3}	6.65×10^{0}	6.40×10^{2}
	Configuration 12		
70	6.41×10^{4}		
77.3		1.72×10^{1}	
77.8			3.59×10^{2}
84.9			2.51×10^{2}
85	3.54×10^{3}		
91.9		2.00×10^{0}	
99.9			1.25×10^{2}
100	3.04×10^{2}		
106.9		2.34×10^{-1}	

z, Distance from Source (cm)	Thermal-Neutron Flux (nv_{th})	Fast-Neutron Dose Rate (mrep/hr)	Gamma-Ray Dose Rate (mr/hr)
	Configuration 13		
100		1.67×10^{0}	6.33×10^{1}
101	1.28×10^{3}		
104	7.71×10^{2}		
108	3.64×10^{2}	4.48×10^{-1}	4.48×10^{1}
123	2.78×10^{1}		2.58×10^{1}
	Configuration 14		
115			1.71×10^{1}
117	2.43×10^{2}		
124	6.13×10^{1}		
124.3			1.21×10^{1}
129	2.54×10^{1}		
129.3			1.00×10^{1}
139	4.85×10^{0}		
139.3			7.10×10^{0}
	Configuration 15		
133			4.74×10^{0}
134	4.18×10^{1}		
142	1.04×10^{1}		
157	8.60×10^{-1}		
	Configuration 16		
147	5.76×10^{0}		
149			2.43×10^{0}
154	1.69×10^{0}		2.07×10^{0}
160	6.22×10^{-1}		1.63×10^{0}

z, Distance from Source (cm)	Thermal-Neutron Flux (nv_{th})	Fast-Neutron Dose Rate (mrep/hr)	Gamma-Ray Dose Rate (mr/hr)
	Configuration 17		
134	1.98×10^{1}		
136			5.49×10^{0}
141.1	6.16×10^{0}		
143.9			4.13×10^{0}
148	2.06×10^{0}		
150			3.34×10^{0}
156.1	6.22×10^{-1}		
158.9			2.26×10^{0}
	Configuration 18		
119			1.56×10^{1}
120	8.95×10^{1}		
127.5			1.09×10^{1}
128	2.44×10^{1}		
132.5			8.87×10^{0}
133	1.02×10^{1}		
142.5			6.28×10^{0}
143	2.28×10^{0}		
	Configuration 19		
107			3.80×10^{1}
108.8		4.30×10^{-1}	
110	2.55×10^{2}		
116	8.91×10^{1}		2.50×10^{1}
131	7.60×10^{0}		1.41×10^{1}
	Configuration 20		
77	1.79×10^{4}		
82		7.66×10^{0}	
84	4.81×10^{3}		
84.2			2.11×10^{2}
91.3	1.24×10^{3}	1.97×10^{0}	1.51×10^{2}
98.3	3.79×10^{2}		1.11×10^{2}
106.3	1.01×10^{2}	2.22×10^{-1}	7.81×10^{1}

z, Distance from Source (cm)	Thermal-Neutron Flux (nv_{th})	Fast-Neutron Dose Rate (mrep/hr)	Gamma-Ray Dose Rate (mr/hr)
	Configuration 21		
54	1.78×10^5		
60		1.14×10^2	
61.8			1.25×10^3
67		3.67×10^1	
68.9	1.34×10^4		8.82×10^2
72		1.88×10^1	
75.9			6.17×10^2
76	4.04×10^3		
82		4.00×10^0	
83.9	1.15×10^3		4.24×10^2
	Configuration 22		
40	1.95×10^6		
45	6.35×10^5		
47			3.93×10^3
55	8.72×10^4		2.54×10^3
60	3.46×10^4		1.97×10^3
65		3.12×10^1	
70	6.21×10^3	1.45×10^1	1.16×10^3
75		7.48×10^0	
80		3.59×10^0	
	Configuration 23		
28.5	8.62×10^6		
35.5	1.77×10^6		
42.6	3.94×10^5		

Appendix B

LIST OF FIGURES

Fig. No.	Title	Page No.
1	Concrete Configurations Tested at the LTSF	5
2	Thermal-Neutron Flux in Water Beyond Configurations 1, 2, 4, and 14 as a Function of Distance from the Source: Comparison of the Attenuation of Adjacent Concrete Slabs in Air and Water Media	9
3	Thermal-Neutron Flux in Water Beyond Configurations 4, 5, 6, and 7 as a Function of Distance from the Source: Effect of Introducing a 1/8- to 1/2-in.-thick Water Gap After Each 2-in.-Thickness of Concrete	10
4	Thermal-Neutron Flux in Water Beyond Configurations 8, 9, 10, 11, 12, 13, 14, and 15 as a Function of Distance from the Source: Effect of Increasing the Total Thickness of Adjacent Concrete Slabs in a Water Medium	11
5	Thermal-Neutron Flux in Water Beyond Configurations 16, 17, 18, 19, 20, 21, 22, and 23: Effect of Introducing a 1/2 in.-thick Water Gap After Each 4-in. Thickness of Concrete	12
6	Thermal-Neutron Flux in Water Beyond Various Thicknesses of a Concrete Shield in a Water Medium	13
7	Thermal-Neutron Flux in Water Beyond Various Thicknesses of a Concrete Shield in Which a 1/2-in.-thick Water Gap Follows Each 4-in. Thickness of Concrete	14
8	Fast-Neutron Dose Rates in Water Beyond Configurations 2, 3, and 4 as a Function of Distance from the Source: Comparison of the Attenuation of Adjacent Concrete Slabs in Air and Water Media	15
9	Fast-Neutron Dose Rates in Water Beyond Configurations 4, 5, 6, and 7 as a Function of Distance from the Source: Effect of Introducing a 1/8-in.- to 1/2-in.-thick Water Gap After Each 2-in. Thickness of Concrete	16
10	Fast-Neutron Dose Rates in Water Beyond Configurations 11, 12, and 13 as a Function of Distance from the Source: Effect of Increasing the Total Thickness of Adjacent Concrete Slabs in a Water Medium	17

Fig. No.	Title	Page No.
11	Fast-Neutron Dose Rates in Water Beyond Configurations 19, 20, 21, and 22 as a Function of Distance from the Source Plate: Effect of Introducing a 1/2-in.-thick Water Gap After Each 4-in. Thickness of Concrete	18
12	Total Macroscopic Neutron Cross Sections for Portland Concrete	20
13	Gamma-Ray Dose Rates in Water Beyond Configurations 1, 2, 3, 4, and 14 as a Function of Distance from the Source: Comparison of the Attenuation of Adjacent Concrete Slabs in Air and Water Media	27
14	Gamma-Ray Dose Rates in Water Beyond Configurations 4, 5, 6, and 7 as a Function of Distance from the Source: Effect of Introducing a 1/8- to 1/2-in.-thick Water Gap After Each 2-in.-Thickness of Concrete	28
15	Gamma-Ray Dose Rates in Water Beyond Configurations 10, 11, 12, 13, 14, and 15 as a Function of Distance from the Source: Effect of Increasing the Total Thickness of Adjacent Concrete Slabs in a Water Medium	29
16	Gamma-Ray Dose Rates Beyond Configurations 16, 17, 18, 19, 20, 21, and 22 as a Function of Distance from the Source: Effect of Introducing a 1/2-in.-thick Water Gap After Each 4-in. Thickness of Concrete	30
17	Gamma-Ray Dose Rates in Water Beyond Various Thicknesses (in inches) of a Concrete Shield	31
18	Gamma-Ray Dose Rates in Water Beyond Various Thicknesses (in inches) of a Concrete Shield in Which a 1/2-in.-thick Water Gap Follows Each 4-in. Thickness of Concrete	32
19	Gamma-Ray Dose Rates in Water Beyond Various Thicknesses (in centimeters) of a Concrete Shield	33
20	Gamma-Ray Dose Rate in Water Beyond Various Thicknesses (in centimeters) of a Concrete Shield in Which a 1/2-in.-thick Water Gap Follows Each 4-in. Thickness of Concrete	34

ORNL-2193
Physics and Mathematics
TID-4500 (13th ed., Rev.)
February 15, 1958

INTERNAL DISTRIBUTION

1. C. E. Center
2. Biology Library
3. Health Physics Library
4-5. Central Research Library
6. Reactor Experimental Engineering Library
7-26. Laboratory Records Department
27. Laboratory Records, ORNL R.C.
28. A. M. Weinberg
29. L. B. Emlet (K-25)
30. J. P. Murray (Y-12)
31. J. A. Swartout
32. E. H. Taylor
33. E. D. Shipley
34. A. H. Snell
35-44. E. P. Blizard
45. M. L. Nelson
46. W. H. Jordan
47. G. E. Boyd
48. R. A. Charpie
49. S. C. Lind
50. F. L. Culler
51. A. Hollaender
52. J. H. Frye, Jr.
53. M. T. Kelley
54. J. L. Fowler
55. R. S. Livingston
56. K. Z. Morgan
57. T. A. Lincoln
58. A. S. Householder
59. C. P. Keim
60. C. S. Harrill
61. C. E. Winters
62. D. S. Billington
63. H. E. Seagren
64. D. Phillips
65. A. J. Miller
66. M. J. Skinner
67. R. R. Dickison
68. J. A. Harvey
69. A. Simon
70. F. C. Maienschein
71. C. E. Clifford
72. A. D. Callihan
73. R. R. Coveyou
74. W. Zobel
75. F. L. Keller
76. C. D. Zerby
77. D. K. Trubey
78. S. K. Penny
79. R. W. Peelle
80. H. M. Glen
81. L. B. Holland
82. L. Jung
83. E. G. Silver
84. A. B. Reynolds
85. G. T. Chapman
86. A. D. Callihan
87. V. R. Cain
88. F. J. Muckenthaler
89. D. Cady
90. R. B. Murray
91-95. J. M. Miller
96. H. Bertini
97. T. V. Blosser
98. K. M. Henry
99. H. Moran
100. S. Terasawa
101. C. A. Preskitt
102. F. L. Friedman (consultant)
103. H. Goldstein (consultant)
104. H. Hurwitz, Jr. (consultant)
105. L. W. Nordheim (consultant)
106. R. R. Wilson (consultant)
107. ORNL - Y-12 Technical Library, Document Reference Section

EXTERNAL DISTRIBUTION

108. R. K. Osborn, Department of Nuclear Engineering, University of Michigan, Ann Arbor, Mich.
109. Harold S. Davis, General Electric Co., Bldg. 762, Richland, Wash.
110. Harold L. Hull, E. I. du Pont de Nemours, du Pont Bldg., Wilmington, Del.
111. R. Aronson, Technical Research Group, New York, N. Y.
112. F. A. Aschenbrenner, General Electric, Cincinnati, Ohio
113. H. E. Hungerford, Atomic Power Development Association, Inc., 1911 First St., Detroit 26, Mich.

114. J. Van Hoomissen, General Electric, Idaho
115. F. N. Watson, Lockheed, Marietta, Ga.
116. M. F. Valerino, General Nuclear Engineering Corp., P. O. Box 245, Dunedin, Fla.
117. J. B. Dee, Pratt & Whitney Aircraft, CANEL Division, East Hartford, Conn.
118. G. J. Rausa, The Martin Company, Baltimore, Md.
119. R. D. Schamberger, Brookhaven National Laboratory
120. Harold H. Rossi, Department of Radiology, Columbia University, 630 West 168th St., New York 38, N. Y.
121. Henry E. Stone, Knolls Atomic Power Laboratory, Bulter Bldg., C-2, P. O. Box 1072, Schenectady, N.Y.
122. L. A. Bowman, WCLJX, Wright-Patterson AFB, Ohio
123. Division of Research and Development, AEC, ORO

24-727. Given distribution as shown in TID-4500 (13th ed., Rev., Feb. 15, 1958) under Physics and Mathematics category (75 copies - OTS)